Int J Appl Earth Obs Geoinformation 89 (2020) 102069

Contents lists available at ScienceDirect

Int J Appl Earth Obs Geoinformation

journal homepage: www.elsevier.com/locate/jag

Effects of varying solar-view geometry and canopy structure on solar-induced chlorophyll fluorescence and PRI

Khelvi Biriukova[a], Marco Celesti[a,*], Anton Evdokimov[a], Javier Pacheco-Labrador[b], Tommaso Julitta[c], Mirco Migliavacca[b], Claudia Giardino[d], Franco Miglietta[e], Roberto Colombo[a], Cinzia Panigada[a], Micol Rossini[a]

[a] Remote Sensing of Environmental Dynamics Laboratory, Department of Earth and Environmental Sciences (DISAT), University of Milano-Bicocca, Piazza della Scienza 1, Milano 20126, Italy
[b] Max Planck Institute for Biogeochemistry, Hans Knöll Straße 10, Jena D-07745, Germany
[c] JB Hyperspectral Devices UG, 40225 Düsseldorf, Germany
[d] Institute for Electromagnetic Sensing of the Environment, National Research Council (IREA-CNR), Via Bassini 15, 20133 Milan, Italy
[e] Institute of BioEconomy, National Research Council (IBE-CNR), Via Caproni 8, 50145 Florence, Italy

ARTICLE INFO

Keywords:
Solar-induced chlorophyll fluorescence
PRI
BRDF
Multi-angular
SCOPE
Hyperspectral

ABSTRACT

The increasing amount of continuous time series of solar-induced fluorescence (SIF) and vegetation indices (e.g. Photochemical Reflectance Index, *PRI*) acquired with high temporal (sub-minute) frequencies is foreseen to allow tracking of the structural and physiological changes of vegetation in a variety of ecosystems. Coupled with observations of CO_2, water, and energy fluxes from eddy covariance flux towers, these measurements can bring new insights into the remote monitoring of ecosystem functioning. However, continuously changing solar-view geometry imposes directional effects on diurnal cycles of the fluorescence radiance in the observation direction (*F*) and *PRI*, controlled by structural and biochemical vegetation properties. An improved understanding of these variations can potentially help to disentangle directional responses of vegetation from physiological ones in the continuous long-term optical measurements and, therefore, allow to deconvolve the physiological information relevant to ecosystem functioning. Moreover, this will also be useful for better interpreting and validating *F* and *PRI* satellite products (e.g., from the upcoming ESA FLEX mission).

Many previous studies focused on the characterization of reflectance directionality, but only a handful of studies investigated directional effects on *F* and vegetation indices related to plant physiology. The aim of this study is to contribute to the understanding of red (F_{687}) and far-red (F_{760}) fluorescence and *PRI* anisotropy based on field spectroscopy data and simulations with the Soil-Canopy Observation of Photochemistry and Energy fluxes (SCOPE) model. We present an extensive dataset of multi-angular measurements of *F* and *PRI* collected at canopy level with a high-resolution instrument (FloX, JB Hyperspectral Devices UG, Germany) over different ecosystems: Mediterranean grassland, alfalfa, chickpea and rice.

We found, that F_{760} and F_{687} directional responses of horizontally homogeneous canopies are characterized by higher values in the backscatter direction with a maximum in the hotspot and lower values in the forward scatter direction. The *PRI* exhibited similar response due to its sensitivity to sunlit-shaded canopy fractions.

As confirmed by radiative transfer forward simulations, we show that in the field measurements leaf inclination distribution function controls the shape of *F* and *PRI* anisotropic response (bowl-like/dome-like shapes), while leaf area index and the ratio of leaf width to canopy height affect the magnitude and the width of the hotspot. Finally, we discuss the implications of off-nadir viewing geometry for continuous ground measurements. *F* observations under oblique viewing angles showed up to 67 % difference compared to nadir observations, therefore, we suggest maintaining nadir viewing geometry for continuous measurements of *F* and vegetation indices. Alternatively, a correction scheme should be developed and tested against multi-angular measurements to properly account for anisotropy of canopy *F* and *PRI* observations. The quantitative characterization of these effects in varying illumination geometries for different canopies that was performed in this study will also be useful for the validation of remote sensing *F* and *PRI* products at different spatial and temporal scales.

* Corresponding author.
E-mail address: marco.celesti@unimib.it (M. Celesti).

https://doi.org/10.1016/j.jag.2020.102069
Received 23 September 2019; Received in revised form 31 January 2020; Accepted 4 February 2020

1. Introduction

In the last decades the remote sensing community has increased its interest in the study of vegetation physiology. Technical advances have enhanced the capabilities to exploit the subtle signals induced by mechanisms related to the downregulation of photosynthesis (Grace et al., 2007; Coops et al., 2010) by means of solar-induced chlorophyll fluorescence (SIF) and the Photochemical Reflectance Index (*PRI*). SIF is a part of photosynthetically active radiation absorbed by chlorophyll (*APAR*) and reemitted at longer wavelengths (red and far-red). SIF competes with photochemical quenching (PQ) and non-photochemical quenching (NPQ) for the same energy and can be considered as a direct probe of the functioning of the photosynthetic machinery (Meroni et al., 2009; Porcar-Castell et al., 2014; Mohammed et al., 2019). In fact, SIF emission is affected not only by variations in the efficiency of PQ, but also of NPQ. This implies that both SIF and NPQ should be taken into account for getting information on the photosynthetic functioning (Porcar-Castell et al., 2014; Frankenberg and Berry, 2018). Highly sensitive to changing environmental conditions, SIF was employed for monitoring variations in photosynthesis and was proved to serve as a better indicator of vegetation stress than traditional reflectance-based indices (Sun et al., 2015; Rossini et al., 2015; Guan et al., 2016; Yang et al., 2017; Luus et al., 2017; Köhler et al., 2018; Migliavacca et al., 2017; Celesti et al., 2018). NPQ is a regulatory mechanism that helps keeping the energy balance of the light-absorbing complexes stable by dissipating the excess of energy as heat, and thus minimizing the chance of formation of harmful reactive species (Krause and Weis, 1991; Müller et al., 2001). The protection of the photosystems from the photoinhibition takes place in the energy-dependent NPQ and it is associated with the de-epoxidation of the xanthophyll pigments (Demmig-Adams and Adams, 1992), that, in turn, results in a decrease in reflectance (*R*) at 531 nm which can be assessed with *PRI* (Gamon et al., 1992; Peñuelas et al., 1995; Middleton et al., 2018).

The link between *PRI* and light-use efficiency (LUE) (Garbulsky et al., 2011) was observed for a number of species using proximal (Filella et al., 1996; Zhang et al., 2015; Alonso et al., 2017), airborne (Rossini et al., 2013; Soudani et al., 2014; Schickling et al., 2016; Middleton et al., 2017) and spaceborne sensors (Drolet et al., 2005; Garbulsky et al., 2013; Stagakis et al., 2014; Middleton et al., 2016). Similarly, in the last years, SIF datasets have been collected over a number of natural and agricultural vegetation targets using ground-based platforms (Cogliati et al., 2015a; Rossini et al., 2016; Campbell et al., 2019), unmanned aerial vehicles (UAVs) (Zarco-Tejada et al., 2012; Garzonio et al., 2017) and airborne platforms (Rascher et al., 2015; Sun et al., 2018; Colombo et al., 2018). In this context, a substantial input was given by the Earth-Explorer 8 FLuorescence EXplorer (FLEX) satellite mission of the European Space Agency (ESA), the first mission specifically intended for global-scale SIF retrieval from space in the red and far-red spectral regions (Drusch et al., 2017). Continuous measurements of fluorescence radiance in the observation direction (*F*) are becoming increasingly available from high spectral resolution devices (Aasen et al., 2019). Among these, the FloX system (JB Hyperspectral Devices UG, Germany) was developed as a ground counterpart for the FLEX optical payload, with intention to gain insights in short-to-long term vegetation processes, and to establish a ground network for validation of the satellite observations (Julitta et al., 2017).

Leaf properties and canopy structure strongly determine the radiative transfer of *F* and *PRI*. Scattering and absorption processes first take place within the leaf and then propagate further throughout the canopy. Within the canopy, the canopy structure (leaf area index (*LAI*), leaf inclination distribution function (*LIDF*) and bidirectional gap fraction) determines multiple scattering and absorption effects between different layers of foliage. Additionally, the canopy structure also affects the *F* and *PRI* values observed under different solar zenith and azimuth angles (*SZA*, *SAA*), view zenith angles (*VZA*) and relative azimuth angles between the sun and the sensor (*RAA*) (Middleton et al., 2012; van der Tol et al., 2009).

These directional effects do not depend exclusively on the fraction of sunlit and shaded leaves observed with a given field of view (FOV), but are also influenced by the physiological response of each observed leaf to different levels of absorbed radiation (Hall et al., 2008; Hilker et al., 2008). Multi-angular observations from the tower-based spectroradiometer AMSPEC over conifer (Hall et al., 2008, 2011; Hilker et al., 2008, 2010a, 2011; Middleton et al., 2009a; Zhang et al., 2015, 2017) and deciduous species (Hilker et al., 2010b), and from the field-based system installed over corn (Middleton et al., 2009b, 2012; Cheng et al., 2010, 2012) demonstrated that *PRI* (computed as $PRI = (R_{531} - R_{570})/(R_{570} + R_{531})$), exhibited lower values near the hot-spot due to higher fraction of sunlit foliage, where the canopy is exposed to the light-excess conditions.

With the proliferation of high-resolution spectrometers, the interest in characterizing *F* anisotropy through multi-angular measurements increased. Middleton et al. (2012) observed that at daily scale *F* retrieved in the O_2-B absorption band (F_{687}) in corn was insensitive to solar-view geometry, while the directional response of *F* retrieved in the O_2-A absorption band (F_{760}) varied for the young and the mature crop. In the early growth stage, F_{760} increased at high *VZA*, while in the mature canopy F_{760} significantly decreased at high *VZA*. Pinto et al. (2017) investigated F_{760} directionality of individual leaf surfaces using imaging spectroscopy and stereo imaging in sugar beet, showing that F_{760} increased with higher viewing angles. Diurnal multi-angular measurements of *F* in the two absorption bands in winter wheat (Liu et al., 2016) revealed the differences in the shapes of *F* distribution in the Solar Principal Plane (SPP) for F_{760} and F_{687}. These differences were attributed to the dominant processes in the two absorption bands — *F* scattering in O_2-A and *F* reabsorption in O_2-B — as well as to the bi-directional gap fraction.

Most of the ground *R* and *F* measurements have been collected at nadir (Daumard et al., 2010; Cogliati et al., 2015a; Yang et al., 2018). However, when the spectrometers are deployed over high forests, the sensor's fiber optics are usually tilted up to 30° off-nadir to avoid having the tower structure in the radiometric footprint or to observe a particular part of the canopy (Yang et al., 2015, 2017; Wohlfahrt et al., 2018). This setup has implications for the comparisons of data over time and space, and for potential calibration and validation (Cal/Val) activities. Several initiatives have aimed to identify the scientific requirements for optical measurement systems for deployment on flux towers, such as SpecNet (http://specnet.info; Gamon et al., 2006), the COST actions EUROSPEC (ES0903) (http://cost-es0903.fem-environment.eu; Balzarolo et al., 2011; Porcar-Castell et al., 2015) and OPTIMISE (ES1309) (http://optimise.dcs.aber.ac.uk; Aasen et al., 2019; Cendrero-Mateo et al., 2019; Pacheco-Labrador et al., 2019). Nevertheless, while the physical processes behind the *F* and *PRI* directionality have been discussed based on modelling (van der Tol et al., 2009; Vilfan et al., 2018) and field observations (Hilker et al., 2008; Liu et al., 2016), the impact of canopy structure and solar-view geometry on both signals simultaneously has not been quantitatively explored.

In this study we measured the anisotropy of F_{760}, F_{687}, and *PRI* during a day with a consistent setup over four vegetation targets characterized by different structure and illumination geometry to address the following specific objectives:

1) to investigate the directional response of *F* and *PRI* and its correlation with *R* combining field data and radiative transfer simulations with the Soil-Canopy Observation of Photochemistry and Energy fluxes (SCOPE) model; 2) to evaluate the impact of the viewing geometry on the time series of spectral measurements of *F* and *PRI* and to provide recommendations on geometrical configuration of optical measurement systems for deployment on flux towers.

2. Materials and methods

2.1. Spectral data collection and study sites

Multi-angular measurements of *F* and *R* were acquired with the FloX system, specifically designed to retrieve fluorescence in the O_2-A (760 nm) and O_2-B (687 nm) absorption bands using a high-resolution QE Pro spectrometer (wavelength range of 650–800 nm, spectral sampling interval (SSI) of 0.17 nm and full width at half maximum (FWHM) of 0.3 nm), and visible-near-infrared (VIS - NIR) reflectance with the Flame spectrometer (wavelength range of 400–950 nm, SSI = 0.65 nm, FWHM = 1.5 nm) (Ocean Optics, USA). Each spectrometer has two channels – one for down-welling irradiance and one for up-welling radiance with a FOV of 25°. Each acquisition cycle consisted of a series of measurements: 1) down-welling irradiance ($E_1^{\downarrow}$), 2) up-welling radiance ($L^{\uparrow}$), 3) a second down-welling irradiance measurement ($E_2^{\downarrow}$), 4) dark current measurement (DC). The second $E_2^{\downarrow}$ measurement allows accounting for the stability of illumination conditions for the subsequent data quality control.

To perform the multi-angular acquisition, FloX was coupled with a goniometer device with a circular base of 160 cm in diameter and the height of 125 cm, allowing to manually vary *VZA* and view azimuth angle (*VAA*) with a step of 5° (Fig. 1) (Giardino and Brivio, 2003). The resulting shape of the target footprint varied from a circle with diameter of 55 cm when observed from nadir to an ellipse with a major axis of 92 cm at extreme *VZA*s. Down-welling irradiance was measured on a calibrated 99 % reflective Spectralon panel (Labsphere Inc., North Sutton, NH, USA), which was fixed and leveled on the tripod and placed 2–3 m away from the goniometer device at the height of 1 m.

F_{760} and F_{687} were estimated using spectral fitting methods (SFM) initially proposed by Meroni and Colombo (2006) and Meroni et al. (2010), and further developed by Cogliati et al. (2015b). *PRI* was computed with the following equation (Gamon et al., 1992):

$$PRI = \frac{R_{570} - R_{531}}{R_{570} + R_{531}} \quad (1)$$

where R_{531} is the reflectance factor of the xanthophyll-sensitive band at 531 nm and R_{570} is reflectance factor of the reference band at 570 nm. With this formulation, *PRI* values can vary between -1 and 1 and are directly proportional to NPQ. In this study, *PRI* was scaled (*sPRI*) according to Rahman et al., 2001 in a range from 0 to 1:

$$sPRI = \frac{PRI + 1}{2} \quad (2)$$

In our study, *sPRI* was chosen to facilitate the comparison of multi-angular observations between different canopies.

Ground spectral measurements were collected in the following horizontally homogeneous canopies (Fig. 1A–C): 1) semiarid grassland constituted by grasses, forbs and legumes (hereafter referred as 'grass') in a Mediterranean tree-grass ecosystem in Majadas de Tiétar, Spain (39°56′24.68″N, 5°45′50.27″W) (Perez-Priego et al., 2015), 2) alfalfa (*Medicago sativa* L.) and 3) chickpea (*Cicer arietinum* L.) fields in Braccagni, Italy (42°49′15.36″N, 11°4′40.49″E). Measurements were also acquired in a row rice canopy (*Oryza sativa* L.) in Braccagni (Fig. 1D). Multi-angular measurements were collected in Majadas de Tiétar from the 20th to the 22nd of March 2018, and in Braccagni from the 5th to the 11th of June 2018 and from the 8th to the 10th of July 2018.

2.2. Spectral measurements protocols

2.2.1. Protocol to characterize the diurnal cycles of the angular distribution of F, sPRI and R

For the definition of the terms used to describe the geometry of spectral measurements please refer to Table 1.

To characterize the diurnal evolution of the angular response of *F*, *sPRI* and *R*, we sampled canopy radiance in the SPP, in which the zenith angular movement of the sensor happens in the plane of the illumination source and the target, and the Cross Principal Plane (CPP), which is perpendicular to the SPP along the azimuthal axis. The predominantly sunlit part of the canopy is observed in the backscatter direction of the SPP (hotspot effect), whereas the shaded fraction is mostly observed in the forward scatter direction of the SPP (coldspot effect) (Fig. 1). One acquisition cycle included measurements in two planes – SPP and CPP. For alfalfa and chickpea, the *VZA* increment was set to 15° resulting in seven observation points from -45° in the backscatter direction to 45° in the forward scatter direction for each plane and a total of 14 observation positions within a cycle. For grass, *VZA* varied from -50° in the backscatter direction to 50° in the forward scatter direction with a step

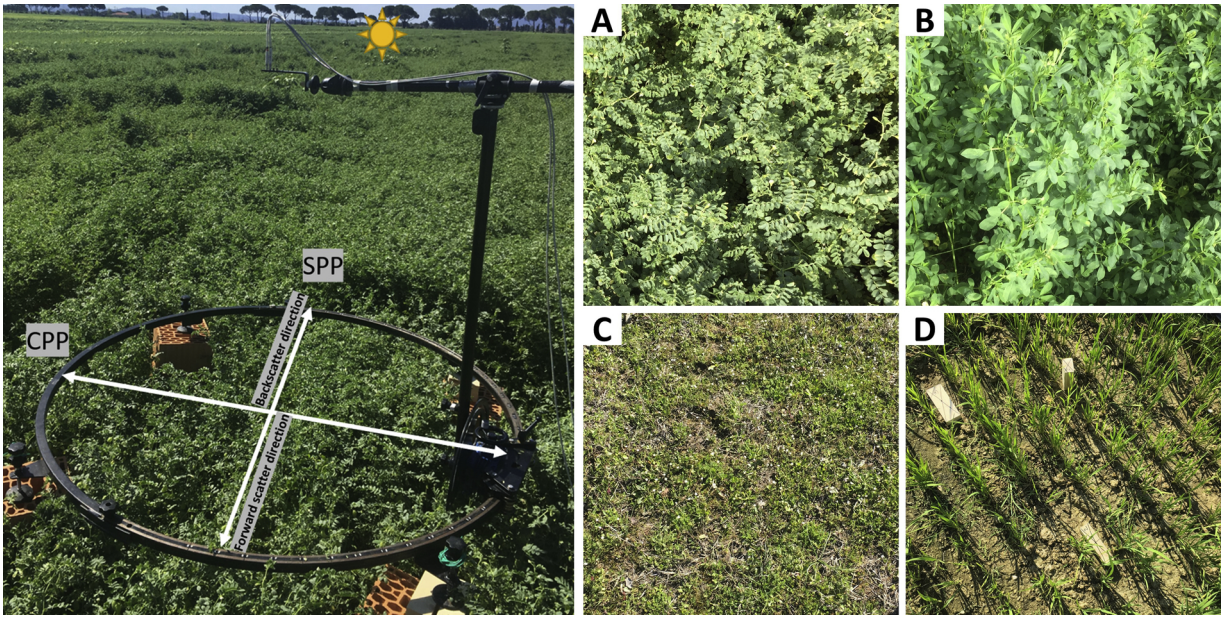

Fig. 1. Left panel: multi-angular spectral measurements of chickpea with the FloX system and the goniometer with schematic representation of the Solar Principal Plane (SPP) with its backscatter and forward scatter directions and Cross Principle Plane (CPP). Right panel: the photographs of studied canopies inside the azimuthal circle of the goniometer device (A – chickpea, B – alfalfa, C – grass, D – rice).

Table 1
Definition of terms used to describe the geometry of the measurements.

SZA	Solar Zenith Angle
SAA	Solar Azimuth Angle
VZA	View Zenith Angle
RAA	Relative Azimuth Angle (relative azimuth angle between the sun and the sensor)
SPP	Solar Principal Plane (angular movement of the sensor sits on the same plane of the illumination source and the target)
CPP	Cross Principal Plane (plane normal to the SPP)
AR	Plane parallel to row direction
CR	Plane perpendicular to row direction
Backscatter direction	Direction of reflected radiation scattering opposite to that of the incident radiation
Forward scatter direction	Direction of reflected radiation scattering coinciding with that of the incident radiation

of 10° and a total of 22 observation positions within a cycle (Table 2). For the rice canopy, we adopted a modified protocol for data acquisition. One acquisition for the row crop included measurements in the SPP and along the row direction (AR) from −45° to 45° with 15° step. During a day, we collected 12–15 acquisition cycles for each canopy. On average, one acquisition cycle took ~15 min with *SZA* changing from 2° to 3.5°. For the diurnal cycles of alfalfa, chickpea and rice at each observation point we acquired three replicates to estimate uncertainties of the measurements by calculating the standard deviation (σ).

2.2.2. Protocol to characterize the angular distribution of F, sPRI and R over the hemisphere

At solar noon, when *SZA* is minimum and changes slowly, we measured several consecutive cycles over four planes starting from the SPP with a step of 45° in azimuth direction and a step of 10° in *VZA* resulting in 44 data points evenly distributed over the hemisphere for chickpea, alfalfa and grass. For the rice canopy, we collected measurements in the SPP, CPP, AR and across the row direction (CR) with the same *VZA* intervals (Table 2). On average, one acquisition cycle took 20 min with *SZA* variation from 0.5° to 1.5°.

2.2.3. Measure of anisotropy

For the characterization of *F* and *sPRI* response to changing solar-view geometry, we used the anisotropy index (*ANIX*) (Sandmeier et al., 1998) to assess the amplitude of the signal variations within a specific plane. Originally, *ANIX* was defined as the ratio of the maximum to the minimum values of reflectance factors. In this study, we adapted the index to *F* and *sPRI*:

$$ANIX_F = \frac{F_{\max}}{F_{\min}} \quad (3)$$

$$ANIX_{sPRI} = \frac{sPRI_{\max}}{sPRI_{\min}} \quad (4)$$

Moreover, for the comparison of the multi-angular observations, *F*, *sPRI* and *R* were normalized between 0 and 1 based on minimum and maximum values measured for each canopy, and the difference between the normalized signals most sensitive to physiology (F_{760}, F_{687} and *sPRI*) and reflectance factors of close bands (R_{750}, R_{680} and R_{570}, respectively) was computed. These differences aim to identify physiological effects in the anisotropy since it is expected that one of the two variables paired to produce these differences is affected by plant physiology, whereas the second is expected to be independent or to be much less affected than the first one. The contribution of fluorescence radiance to the reflectance factor is negligible, considering that R_{750} and R_{680} are outside the oxygen absorption bands, and significant divergences might be interpreted as influence of physiology.

To evaluate the impact of the viewing geometry on the long-term time series of *F* and *PRI*, we computed daily averages of apparent fluorescence yield (*Fy**) and *sPRI* acquired with the same viewing geometry. *Fy** was computed as *F* divided by *PAR* (W m^{-2}).

2.3. Acquisition of biochemical and structural parameters

Biochemical and structural characteristics of vegetation targets are summarized in Table 3. The *LAI* values of the alfalfa and chickpea plots were measured with the LAI-2000 Plant Canopy Analyzer (Li-COR, USA) device under diffuse illumination sky conditions at low solar elevation to exclude the effects of direct sunlight on the sensor. A single *LAI* value for each plot was calculated by averaging 5 measurements collected on 3 transects. The *LAI* value of the rice plot was estimated using hemispherical photos analyzed with the software CAN-EYE (https://www6.paca.inra.fr/can-eye). The *LAI* value of grass was assigned based on the published data at the same experimental site (Migliavacca et al., 2017). The type of *LIDF* (De Wit, 1965) of each canopy was assigned based on the literature and visual interpretation. Leaf chlorophyll content (C_{ab}) of alfalfa and chickpea was determined spectrophotometrically (V-630 UV–Vis, Jasco, Germany) in a 100 % methanol extract at wavelengths 665.2 nm and 652.4 nm, while turbidity was checked by measuring the absorbance at 750 nm and 520 nm. The concentration (μg/ml) for C_{ab} was calculated according to empirical equations by Lichtenthaler and Buschmann (2001). C_{ab} of grass and rice samples was estimated following the pigment extraction protocol by Gonzalez-Cascón and Martín (2018). The hot spot size parameter (*sl*) introduced by Verhoef (1998) in the SAILH canopy reflectance model to describe the hot spot effect for a single layer canopy was computed as the ratio between leaf width (*lw*) and canopy height (*hc*) measured in the field:

$$sl = lw/hc \quad (5)$$

Smaller *sl* factor leads to a sharper hotspot peak, while higher *sl* results in a broader hotspot peak (Jupp and Strahler, 1991).

Table 2
Data acquisition schemes for diurnal and midday cycles for each canopy. Negative values of *VZA* represent the backscatter direction, positive – the forward scatter direction within a plane.

		Chickpea	Alfalfa	Grass	Rice
Diurnal cycles	**N of replicates**	3	3	1	3
	VZA	from −45° to 45°, 15° step	from −45° to 45°, 15° step	from −50° to 50°, 10° step	from −45° to 45°, 15° step
	Azimuth planes	SPP, CPP	SPP, CPP	SPP, CPP	SPP, AR
Midday cycles	**N of replicates**	1			
	VZA	from −50° to 50°, 10° step			
	Azimuth planes	SPP, CPP, ± 45°			SPP, CPP, AR, CR

Table 3
Biochemical and structural characteristics of vegetation targets.

Canopy	Date	*LAI* ($m^2\,m^{-2}$)	*LIDF*	C_{ab} ($\mu g\,cm^{-2}$)	*lw* (m)	*hc* (m)	*sl*
Chickpea	10/06/2018	8	Planophile	36	0.01	0.85	0.01
Alfalfa	6/06/2018 11/06/2018	7	Plagiophile (Walter-Shea et al., 1997)	39.8	0.009	0.80	0.01
Grass	21/03/2018 22/03/2018	1	Spherical (Migliavacca et al., 2017)	39	0.01	0.10	0.1
Rice	10/07/2018	1.95	Erectophile	27	0.01	0.35	0.03

2.4. Simulations of spectro-directional response of F

SCOPE model (v1.73) was used to characterize the effects of canopy structural parameters (*LAI*, *LIDF*, *sl*), C_{ab} and *SZA* on spectro-directional *F* response. SCOPE (van der Tol et al., 2009) is a vertical (1-D) integrated radiative transfer and energy balance model, which calculates radiation transfer in a multilayer canopy in order to obtain reflectance and fluorescence estimations in the observation direction as a function of the *SZA* and *LIDF*. The parameters used for SCOPE simulations are reported in Table 4.

3. Results

3.1. Diurnal changes of the angular distribution of F, sPRI and R in the SPP, CPP and AR

Figs. 2–7 show results of the diurnal measurements of R_{750}, R_{680}, R_{570}, F_{760}, F_{687}, *sPRI* and the differences F_{760} - R_{750}, F_{687} - R_{680}, *sPRI* - R_{570} as a function of *SZA* (*y*-axis) and *VZA* (*x*-axis) in the SPP, CPP and AR planes. The values of *ANIX* computed for *F* and *sPRI* are reported in Tables S1–S6.

3.1.1. Chickpea: F, sPRI and R in the SPP and CPP

R, *F* and *sPRI* acquired in the SPP over chickpea exhibited a dome-like shape with the highest values measured in the backscatter direction (Fig. 2). The hotspot effect was observed for *R*, *F* and *sPRI*. Its location was changing during the day according to the sun position. The highest values of *F* were recorded in the hotspot during midday cycles (*SZA* from -30° to 30°). *F*exhibited an asymmetric diurnal course with lower values in the afternoon compared to the morning values measured at nadir under the same *SZA*. *sPRI*, instead, showed an asymmetric behavior with respect to solar noon with higher values in the morning compared to the afternoon. The hotspot effect of *R* was less pronounced and more localized compared to *F* and *sPRI*. *R* increased at higher *SZA* in the morning and afternoon (*SZA* = −50°; 60°) with respect to the noon. Based on the difference between scaled *F* and *R*, relatively higher *R* was observed at high *SZA* and extreme *VZA* in the backscatter and forward scatter directions, while *F* was higher close to midday and under lower *VZA*. The difference *sPRI* – R_{570} displayed a similar pattern, except for the forward scatter direction, where *sPRI* exhibited values higher than R_{570}.

In the CPP, *R*, *F* and *sPRI* were more evenly distributed and less affected by the viewing geometry compared to the SPP (Fig. 3). A dome-like shape of multi angular *F* measurements can be observed only around midday (*SZA* from −30° to 30°) with the maximum values measured at *VZA* = -15°. Both *F* and *sPRI* showed lower values in the afternoon than in the morning at the same *SZA*. Reflectance factors showed the lowest values in the afternoon when measured at *VZA* from -15° to -45°. The differences F_{760} - R_{750} and F_{687} - R_{680} were positive for all *SZA* and *VZA* combinations except for a stripe in the afternoon cycles (*SZA* from 60° to 65°).

3.1.2. Grass: F, sPRI and R in the SPP and CPP

The distribution of F_{760} for grass showed a bowl-like shape along the SPP with the maximum values acquired at the extreme *VZA* in the backscatter direction and with a clear hotspot effect observed at noon (*SZA* = -39°) at *VZA* between 40° and 50° (Fig. 4). F_{760} measured at nadir showed asymmetric diurnal cycle with slightly higher values in the afternoon, while the diurnal course of *PAR* was symmetrical with respect to solar noon (Fig. S1). The diurnal cycle of *sPRI* measured over grass exhibited higher values in the morning compared to the afternoon. F_{687} and *sPRI* exhibited strong fluctuations in multi-angular measurements, however, an increase was observed in the backscatter direction. Reflectance factors displayed a smooth increase from the forward scatter to backscatter direction with a maximum observed at high *SZA* (−60°; 60°) and *VZA* (−50°). The contrasting behavior of F_{760} and R_{750} were observed early in the morning (*SZA* from −60° to −50°) and late in the afternoon (*SZA* from 50° to 60°) under high *VZA*, when R_{750} exhibited an increase. F_{760}, in turn, showed relatively higher values around noon and at lower *VZA* (from −30° to 30°) compared to R_{750}. The difference F_{687} – R_{680} did not reveal a clear pattern due to high intrinsic variability of F_{687}. In comparison to R_{570}, *sPRI* showed stronger variations with higher values in the forward scatter direction.

Due to lack of the measurements between *SZA* of 40° and 50° in the CPP, it is hard to analyze the diurnal changes in anisotropy of *R*, *F* and *sPRI* over the grass (Fig. 5). Both F_{760} and F_{687} exhibited a bowl-like shape along the CPP for most of the cycles, while F_{687} was characterized by a slightly higher variability within the plane (Tables S3, S4). *sPRI* showed a patchy pattern. Reflectance factors showed little angular variation with slightly higher values observed from oblique *VZA* (−50°; 50°). The difference between F_{760} and R_{750} showed that R_{750} was relatively higher than F_{760} in the morning (*SZA* from −58° to −50°) compared to the afternoon.

3.1.3. Rice: F, sPRI and R in the SPP and AR

The distribution of F_{760} obtained over rice exhibited a similar shape to the one of chickpea in the SPP, with the hotspot in the backscatter direction and the maximum values occurring at noon cycles (*SZA* from -20° to 30°) at *VZA* from -15° to -30° (Fig. 6). The angular distribution of F_{687} was heterogeneous, with a general increase towards high *VZA* in the backscatter direction.

The variation of F_{687} within a plane was generally higher compared to F_{760}, with *ANIX* changing from 2 to 35 in the SPP (Table S5). The *sPRI* directional response differed from the ones measured over horizontally homogeneous canopies. *sPRI* exhibited a dome-like shape with the maximum measured at nadir and in the forward scatter direction,

Table 4
SCOPE model parameters used to simulate spectro-directional response of *F*.

Parameter	Value	Unit
Leaf Area Index (*LAI*)	1, 3, 5, 7	$m^2\,m^{-2}$
Leaf width (*lw*)	0.01, 0.05, 0.1	m
Canopy height (*hc*)	0.1, 0.5, 1	m
Chlorophyll content (C_{ab})	20, 40, 60	$\mu g\,cm^{-2}$
LIDF types	planophile, erectophile, spherical	
Sun zenith angle (*SZA*)	0, 15, 30, 45, 60, 75	deg
View zenith angle (*VZA*)	0, 15, 30, 45, 50, 75	deg
Relative azimuth angles between the sun and an observer (*RAA*)	0, 30, 60, 90, 120, 150,180	deg

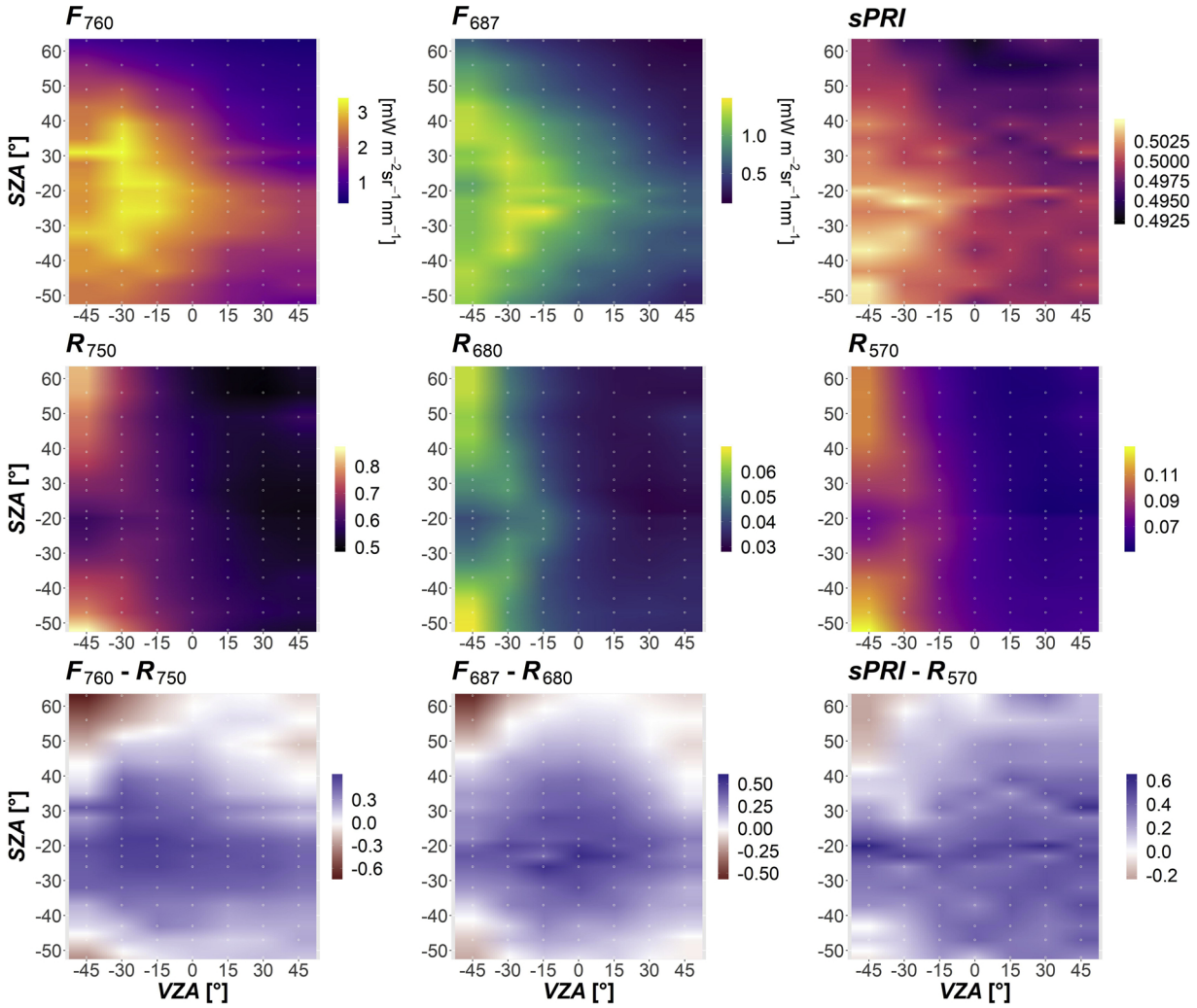

Fig. 2. For chickpea in the SPP: the distribution of F_{760}, F_{687}, *sPRI* (row 1), R_{750}, R_{680}, R_{570} (row 2) and F_{760} - R_{750}, F_{687} - R_{680}, *sPRI* - R_{570} (row 3) as a function of *SZA* and *VZA*. *F*, *sPRI* and *R* were scaled between 0 and 1 before subtraction. Negative values of *SZA* correspond to the cycles acquired before midday, positive - after midday. Negative values of *VZA* represent the backscatter direction, positive – the forward scatter direction within a plane. The points of measurements are marked with white points. The values between the measurements are linearly interpolated.

with the highest values in the afternoon (*SZA* from 30° to 50°). R_{680} and especially R_{570} showed a more distinct hotspot effect than chickpea and grass. R_{750}, in turn, showed a smooth increase from the forward scatter to backscatter direction with maximum values measured at the highest *SZA* (−50°; 60°) and *VZA* = −45°. The difference between F_{760} and R_{750} revealed that generally F_{760} was relatively higher compared to R_{750}, especially in the backscatter direction. The relative difference F_{687} - R_{680}, instead, was negative in the backscatter direction and up to *VZA* = 30° in the forward scatter direction. *sPRI* and R_{570} demonstrated contrasting behavior with their difference being negative in the backscatter at *VZA* from −15° to −45° throughout the day and positive in the forward scatter direction.

When measured in the AR direction, F_{760} had a less evident hotspot and showed a moderate increase towards higher *VZA* compared to the SPP (Fig. 7). F_{687} exhibited an irregular pattern along the plane with a general increase towards the backscatter. *sPRI* measured in AR had a similar behavior to the SPP. Reflectance factors exhibited an asymmetric diurnal cycle with lower values in the morning compared to the afternoon and a maximum found in the backscatter at *SZA* = 40° for R_{680} and R_{570} and at *SZA* = 68° for R_{750}. The difference F_{760} - R_{750} was negative in the afternoon at *SZA* > 50°, while at midday and in the morning the positive values prevailed. The difference between F_{687} and R_{680} showed an opposite pattern – negative values in the morning and midday and positive in the afternoon. The difference between *sPRI* and R_{570} showed an irregular pattern, where *sPRI* was generally relatively higher at all viewing angles except for a stripe of nadir measurements.

3.2. Midday cycles

In homogeneous canopies (chickpea, alfalfa, grass), the angular distribution of both F_{760} and F_{687} measured in four planes resembled the one of reflectance - exhibiting smooth surfaces with gradually increasing values towards the backscatter direction and decreasing towards the forward scatter direction (polar plots, Fig. 8). The angular distribution of *F* measured in rice canopy showed more complex patterns. An evident stripe of high values parallel to the row orientation was observed in F_{760} distribution, while F_{687} exhibited a bowl-like shape with lowest values measured from nadir and in the forward scatter direction at *VZA* = 20° - 30°.

The highest values of *sPRI* in chickpea were acquired in the backscatter and the lowest at *RAA* of 270° in the CPP. Less evident, this pattern was also observed for grass. In alfalfa, the distribution of *sPRI* showed an irregular pattern, with local increases in the CPP at *VZA* of 50°, and close to nadir between *VZA* of 10° and 30°. In rice canopy, there was a pronounced high value stripe along the CPP with the maximum at low *VZA* (10° - 20°) in the forward scatter direction. The

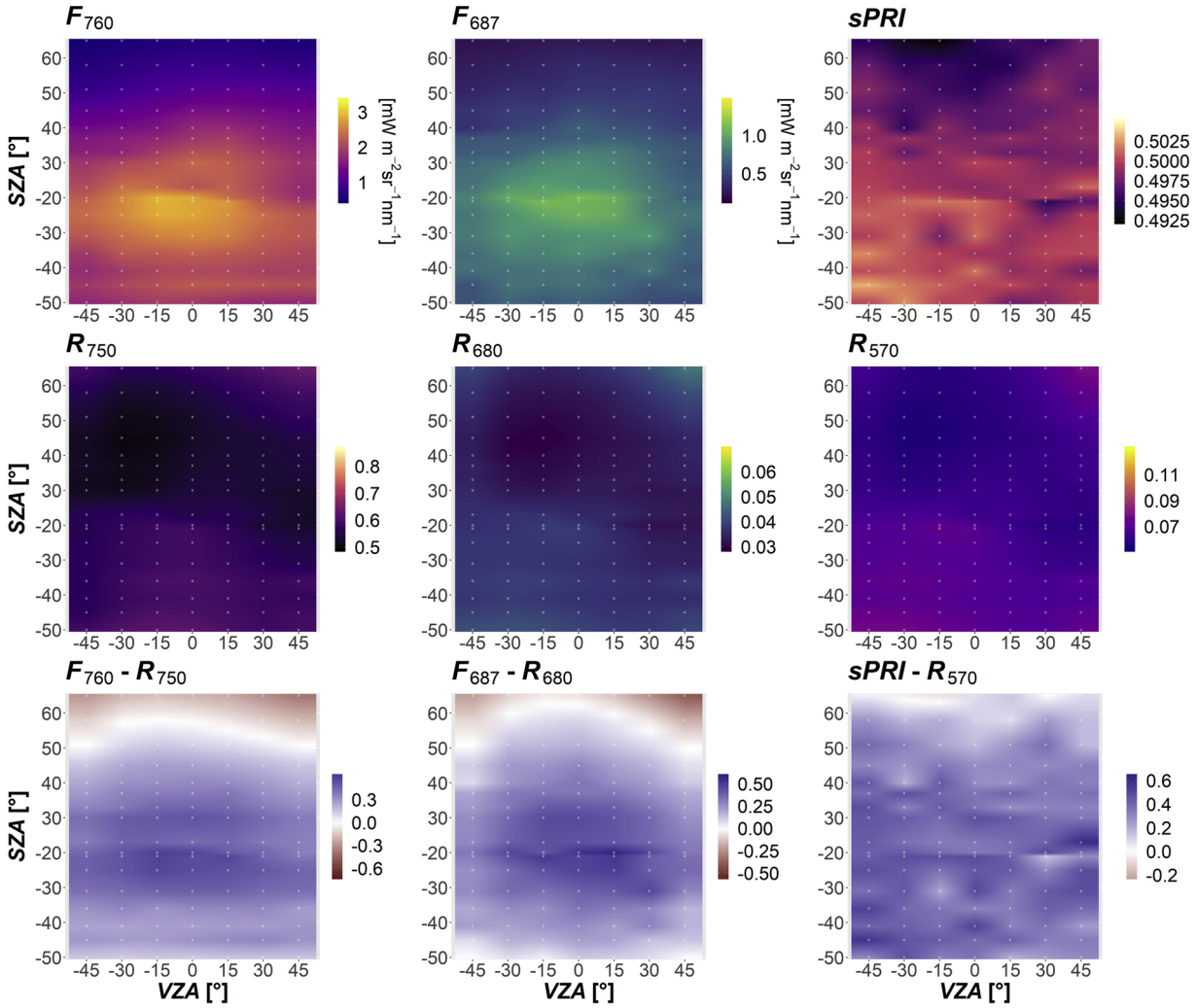

Fig. 3. For chickpea in the CPP: the distribution of F_{760}, F_{687}, *sPRI* (row 1), R_{750}, R_{680}, R_{570} (row 2) and F_{760} - R_{750}, F_{687} - R_{680}, *sPRI* - R_{570} (row 3) as a function of *SZA* and *VZA*. *F*, *sPRI* and *R* were scaled between 0 and 1 before subtraction. Negative values of *SZA* correspond to the cycles acquired before midday, positive - after midday. Negative values of *VZA* represent the backscatter direction, positive - the forward scatter direction within a plane. The points of measurements are marked with white circles. The values between the measurements are linearly interpolated.

lowest *sPRI* values for rice were obtained at *VZA* = 40°–50°.

3.3. Effects of canopy structure on F_{760} and F_{687} directional response in the SPP

3.3.1. Modelling results

For a fixed *SZA* SCOPE model showed that the shape of F_{760} and F_{687} directional response in the SPP is mostly driven by *LIDF* (Fig. S2). In the simulations, F_{760} and F_{687} exhibited a bowl-like shape for erectophile canopy, while *F* showed a distinct increase in the hotspot for planophile and spherical canopy types. *F* of planophile canopy showed a decrease towards higher *VZA*, while *F* of spherical canopy exhibited an increase at extreme *VZA*s forming a more bowl-like shape (Fig. S2).

For a fixed *SZA* the model also describes that *LAI* variations affect the absolute values as well as the shape of the angular distribution of *F* in the SPP. In simulations of increasing *LAI* value, the magnitude of the hotspot increased for planophile and spherical canopy types for both F_{760} and F_{687}. For the erectophile type, F_{760} at *VZA* = 0° declined with increasing *LAI*, while F_{687} exhibited a clear hotspot effect with *LAI* > 3 $m^2 m^{-2}$ (Fig. S3). The highest *ANIX* = 4.4 was observed for F_{687} of the erectophile canopy type with *LAI* = 1 $m^2 m^{-2}$. The planophile canopy type was characterized by the smallest *ANIX* for both F_{760} and F_{687} (Table S7).

SCOPE shows that the width of the region around the hotspot point is driven by the *sl* parameter in planophile, spherical and erectophile canopy types for both F_{760} and F_{687}. With decreasing *sl*, the hotspot peak became sharper (Fig. S4). For *sl* = 1, the hotspot effect in F_{760} and F_{687} angular distribution was significantly broadened and smoothed out in the case of erectophile and spherical canopy types. The effect of *lw* on the shape of *F* directional response was negligible for all canopy types. Canopy height variation only affected the amplitude of the hotspot effect in planophile and spherical canopy type, causing the peak leveling off at *hc* = 0.1 m.

In SCOPE, *SZA* also plays an important role in the shape of *F* directional response (Fig. S5). For planophile canopy type, the hotspot position shifted towards the *VZA* coinciding with the *SZA*. For spherical canopy type, with *SZA* increase, the slope of the angular distribution becomes steeper towards higher *VZA*. *SZA* had the biggest impact on the shape of F_{687} directional response for erectophile canopy with *ANIX* reaching 15.7 at *SZA* = 75° (Table S9).

3.3.2. Comparison between F directional responses of canopies with different structural properties

Both F_{760} and F_{687} directional response for alfalfa and chickpea showed a dome-like shape with maximum values measured in the hotspot at *VZA* = 30° and *SZA* = 22° - 30° during the acquisitions

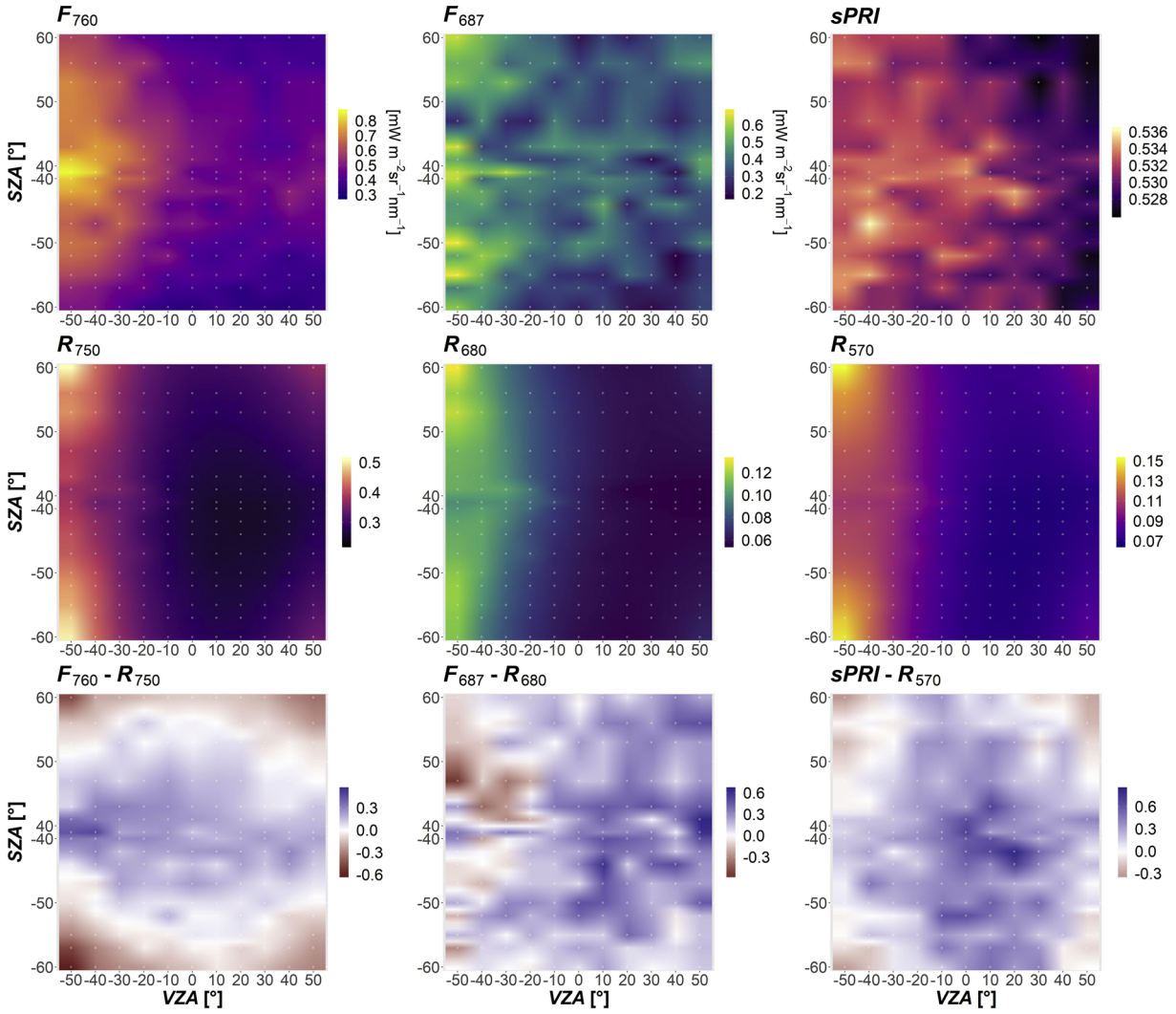

Fig. 4. For grass in the SPP: the distribution of F_{760}, F_{687}, *sPRI* (row 1), R_{750}, R_{680}, R_{570} (row 2), and F_{760} - R_{750}, F_{687} - R_{680}, *sPRI* - R_{570} (row 3) as a function of *SZA* and *VZA*. *F*, *sPRI* and *R* were scaled between 0 and 1 before subtraction. Negative values of *SZA* correspond to the cycles acquired before midday, positive - after midday. Negative values of *VZA* represent the backscatter direction, positive - the forward scatter direction within a plane. The points of measurements are marked with white circles. The values between the measurements are linearly interpolated.

(Fig. 9). *F* measured in alfalfa was higher compared to chickpea. In the forward scatter direction, F_{760} measured in chickpea exhibited a more pronounced coldspot effect decreasing down to 1.06 mW m^{-2} nm^{-1} at *VZA* of 45°. The F_{760} directional distribution in the SPP measured for grass exhibited a bowl-like shape with steeper increase in the backscatter direction. F_{687} values for grass measured along the SPP were slightly lower, more scattered, and showed an increasing trend from the forward scatter to backscatter direction. F_{760} directional response for rice exhibited a pronounced hotspot at *VZA* = -20°, while F_{687} showed a bowl-like pattern with some fluctuations.

3.4. Fluorescence apparent yield and sPRI daily averages

Fy^*_{760} and Fy^*_{687} were generally higher at lower *VZA* at all *RAA* for the chickpea (Fig. 10). The highest values of Fy^*_{760} and Fy^*_{687} were observed at *RAA* = 0° (hotspot) and the lowest at *RAA* = 180° (coldspot). Chickpea *sPRI* also exhibited significant variations, characterized by a decrease at *RAA* = 180° (coldspot) and an increase at 0° (hotspot).

Grass *Fy** and *sPRI* daily averages exhibited inverse patterns compared to chickpea. The maximum values of Fy^*_{760} and *sPRI* corresponded to the highest measured *VZA* = 45°. Fy^*_{760} daily average showed its maximum in the hotspot (*RAA* = 0°) and minimum in the coldspot (*RAA* = 180°) for all measured *VZA*s. Fy^*_{687} daily average increased at *RAA* = 0° and 270° as well. Interestingly, with higher *VZA*s, *Fy** increase at *RAA* = 270° became more pronounced. Similarly to chickpea, grass *sPRI* showed the lowest values in the coldspot and the highest values in the hotspot direction.

Daily averages of *Fy** and *sPRI* measured over rice showed the highest variability among the studied canopies. In most of the cases, the highest Fy^*_{760} values were associated with the hotspot (*RAA* = 0°) and the lowest with the coldspot (*RAA* = 180°). However, Fy^*_{760} signal measured at *VZA* = 45° showed a distinct decrease at *RAA* = 90° (CPP) and the highest values at *RAA* = 0° and 270°. *sPRI* values measured for rice showed an increase at lower *VZA*s, but did not vary substantially as a function of *RAA*.

4. Discussion

4.1. F and sPRI anisotropy as a function of solar-view geometry

Different crops showed diverse shapes of *F*, *sPRI* and *R* angular distribution as an effect of canopy structure and leaf orientation in varying illumination conditions during the day. In particular, the asymmetric diurnal course of both *F* and *PRI* with respect to solar noon

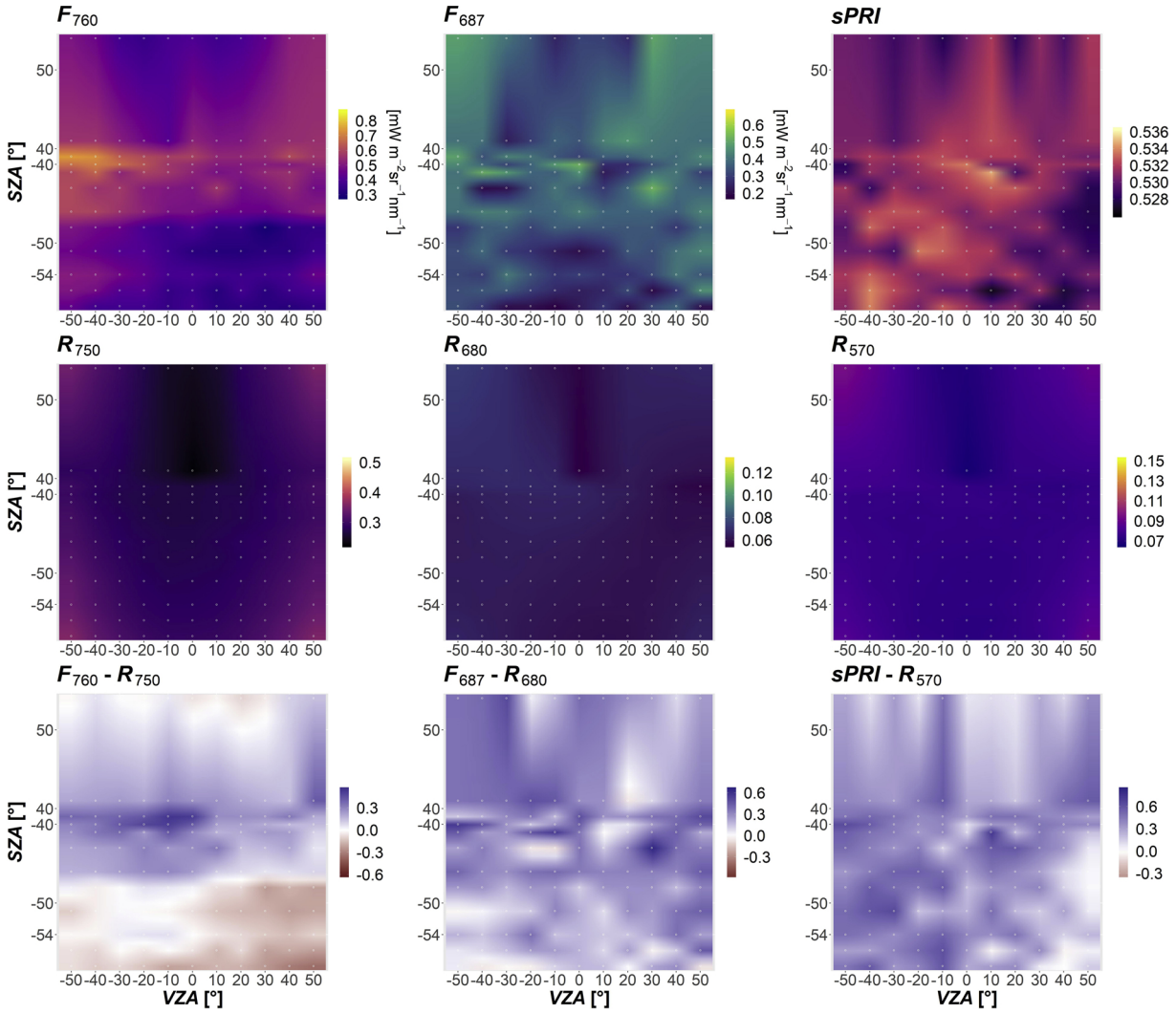

Fig. 5. For grass in the CPP: the distribution of F_{760}, F_{687}, *sPRI* (row 1), R_{750}, R_{680}, R_{570} (row 2), and F_{760} - R_{750}, F_{687} - R_{680}, *sPRI* - R_{570} (row 3) as a function of *SZA* and *VZA*. *F*, *sPRI* and *R* were scaled between 0 and 1 before subtraction. Negative values of *SZA* correspond to the cycles acquired before midday, positive - after midday. Negative values of *VZA* represent the backscatter direction, positive - the forward scatter direction within a plane. The points of measurements are marked with white circles. The values between the measurements are linearly interpolated.

does not always suggest a larger photosynthetic stress in the afternoon (Rascher et al., 2009; Paul-Limoges et al., 2018) as it would be expected (Fig. S1). This fact can be partly attributed to local changes in the proportion of sunlit and shaded leaves inside the canopy induced by changing *SZA* during a day (Damm et al., 2015). Moreover, in the case of chickpea, this behavior might be partly driven by slightly lower *PAR* values in the afternoon compared to the morning (considering the same *SZA*) (Fig. S1). Regarding the effects of varying viewing geometry, the anisotropic response of *F* can be explained by changing canopy depths, from which the photons escape the canopy in the direction of the sensor. When measured under high *VZA*, the sensor captures the signal mostly from the upper sunlit canopy layers and less from deep shaded layers. The canopy structure controls the scattering and absorption of the light inside the canopy (Knyazikhin et al., 2013), resulting in contrasting *F* directional responses for different canopies (Fournier et al., 2012; Damm et al., 2015). For homogeneous canopies, F_{760} in the SPP is higher in the backscatter than in the forward scatter direction with a dome-like shape in chickpea and a bowl-like in grass (Figs. 2, 4). F_{687} has a similar shape to F_{760} with higher variability (higher *ANIX*). This higher variability can be attributed to the prevailing reabsorption by photosynthetic pigments in the red region (Gitelson et al., 1999; Buschmann, 2007; Porcar-Castell et al., 2014), which enhances the directional response of F_{687}. *F* and *R* anisotropy responses are more coordinated in the SPP, where the backscatter and forward scatter directions are characterized by stronger differences in observed sunlit-shaded fraction than other planes. However, in the case of chickpea and grass, *R* tends to have higher hotspot values in the morning and afternoon compared to midday, while the hotspot values of *F* are the highest at midday (Figs. 2, 4). This contrasting behavior might be due to the different nature of these two signals. *R* is a relative metric of scattered radiance normalized by the incoming one. Its anisotropy is purely driven by the radiative transfer of the light scattered by the leaf and within the canopy (which tends to maximize under extreme *SZA*s and *VZA*s due to volumetric scattering; Roujean et al., 1992; Sandmeier et al., 1998). Contrarily, *F* is an absolute variable in part proportional to the amount of incoming radiance, for this reason, *F* maximizes at solar noon.

F anisotropy is less pronounced in the CPP compared to SPP, as the sunlit-shaded fraction of observed leaves varies less due to solar-view geometry. Although for chickpea *F* values measured from oblique *VZA* in the CPP do not deviate a lot from the values acquired from nadir, we observed a peculiar increase at *VZA* between -15° and 15° and *SZA* between 20° and 26° (Fig. 3). This increase could be attributed to the planophile structure of chickpea, characterized by an average leaf angle

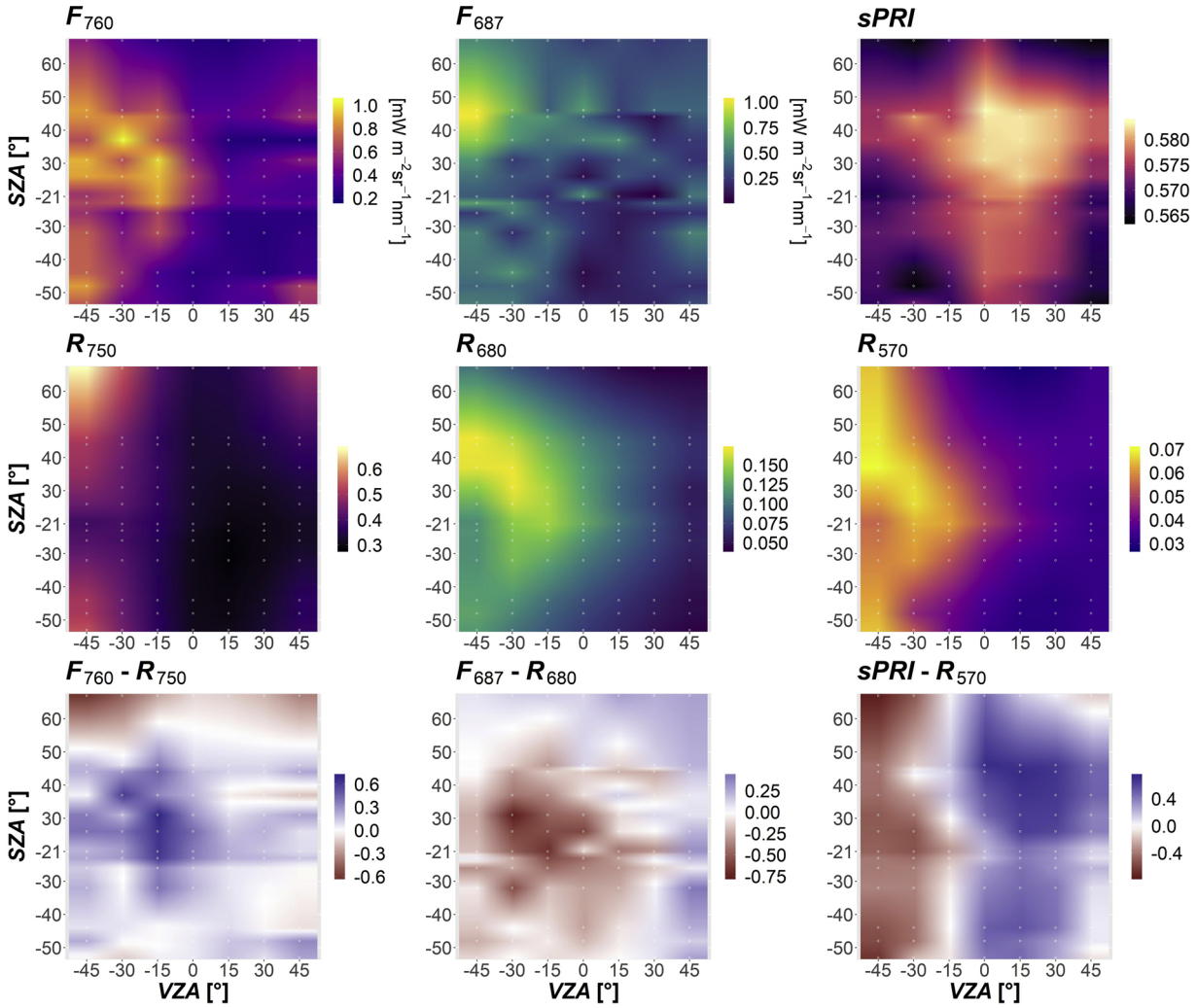

Fig. 6. For rice in the SPP: the distribution of F_{760}, F_{687}, *sPRI* (row 1), R_{750}, R_{680}, R_{570} (row 2), and F_{760} - R_{750}, F_{687} - R_{680}, *sPRI* - R_{570} (row 3) as a function of *SZA* and *VZA*. *F*, *sPRI* and *R* were scaled between 0 and 1 before subtraction. Negative values of *SZA* correspond to the cycles acquired before midday, positive - after midday. Negative values of *VZA* represent the backscatter direction, positive - the forward scatter direction within a plane. The points of measurements are marked with white circles. The values between the measurements are linearly interpolated.

(ALA) of 26° (Zarco-Tejada, 2000). In this case, the sun light is perpendicular to the ALA, resulting in a higher proportion of sunlit leaves observed by the sensor under the corresponding solar-view geometry.

For chickpea, the decrease of *R* in the CPP in the afternoon (Fig. 3) might be explained by the higher fraction of the shaded leaves due to the differences in the canopy height within the footpint. While the *R* response to shadows in the canopy was evident, *F* did not decrease significantly, which suggests that *F* is less affected by the local geometric effects inside the canopy. This might be explained by the fact that *F* signal at leaf level is characterized by isotropic emission (Yang and van der Tol, 2018), which in some cases might result in a less strong angular response than *R*. Moreover, the link between the incoming radiance and the *F* emission is mediated by the different physiological state of the leaves in the shaded/illuminated portions of the canopy.

For the homogenous canopies (chickpea and grass), *sPRI* directional response in the SPP is characterized by a decrease in the forward scatter direction and an increase in the backscatter direction (Figs. 2, 4). Such variability is driven by the dominance of sunlit leaves fraction observed in the backscatter direction, where photoprotective mechanisms activated under higher light intensity cause higher *sPRI* values (Gamon et al., 1992) compared to the values measured in the forward scatter direction with higher shaded fraction. These results are consistent with the previous research on *PRI* directional response in coniferous forests (Hilker et al., 2008; Hall et al., 2008; Zhang et al., 2015, 2017) and in cornfields (Middleton et al., 2012; Cheng et al., 2010, 2012). Midday *sPRI* values acquired from nadir conform with typical values associated with high light conditions found in the literature (from 0.45 to 0.5; Rossini et al., 2010; Perez-Priego et al., 2015; Schickling et al., 2016).

For rice, *F* variability within the SPP was particularly strong (Table S5) due to the high contrast between nadir and off-nadir observations determined by the erectophile canopy type. At *VZA* = 0° the reflected radiance mostly originates from the less illuminated canopy levels, while with increasing *VZA*s the contribution of well-illuminated top layers of vegetation to the signal proportionally increases (Sandmeier et al., 1998). When the sun elevation increases, the hotspot effect of F_{760} becomes more distinct; however, its position does not always correspond to *SZA* (Fig. 6). The shift of the hotspot to lower *VZA* (15° - 30°) observed for several cycles (Fig. 6) can be attributed to complex interactions between canopy leaf angles and observation geometry, resulting in the maximum of vegetated fraction within the footprint at this particular viewing geometry.

When observing the canopy along the row direction, the general increase of *F* in the backscatter direction is preserved (Fig. 7), which can be explained by a higher probability of having more sunlit fraction observed through the space between rows (Zhao et al., 2010). Lower

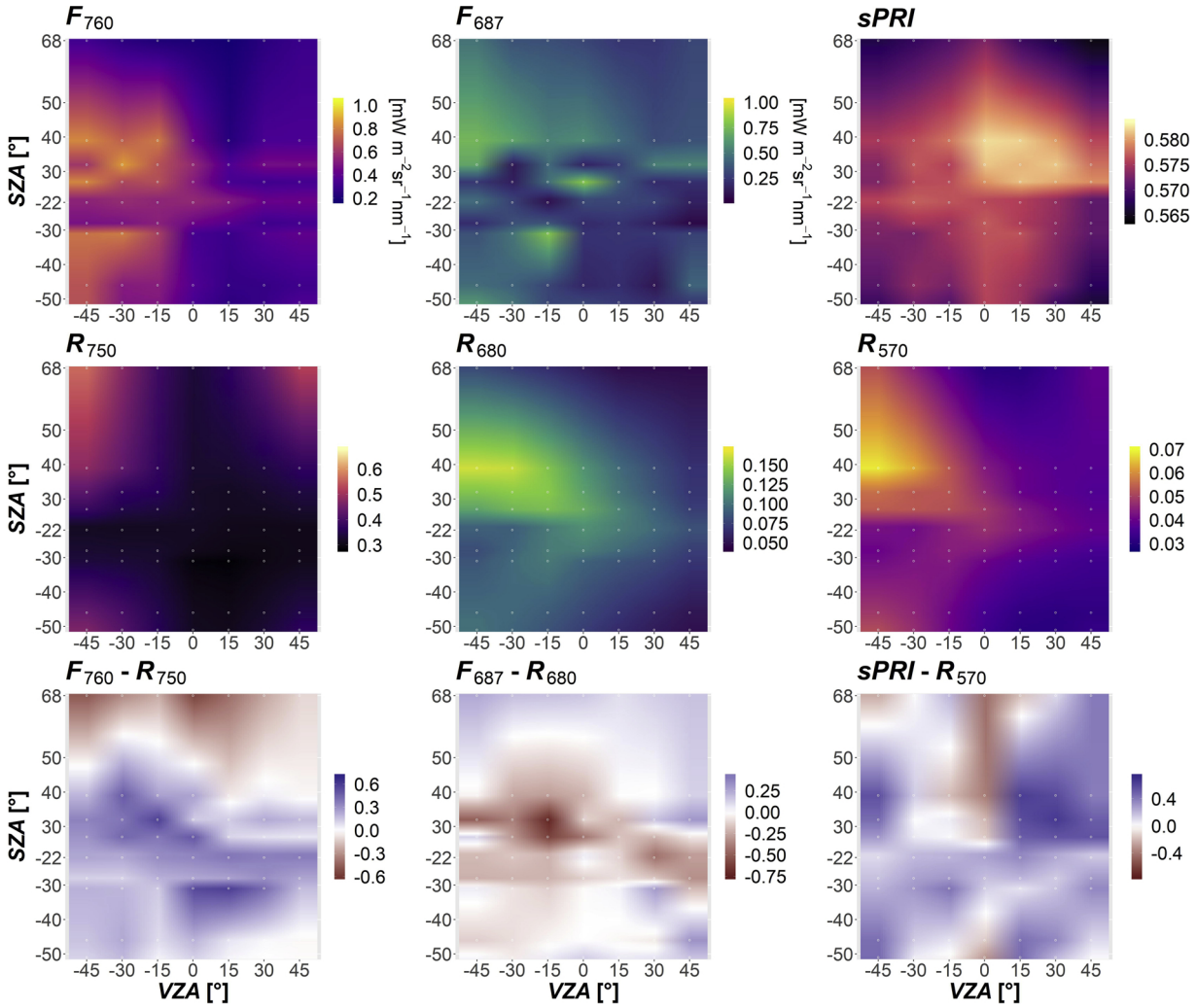

Fig. 7. For rice in the AR: the distribution of F_{760}, F_{687}, *sPRI* (row 1), R_{750}, R_{680}, R_{570} (row 2), and F_{760} - R_{750}, F_{687} - R_{680}, *sPRI* - R_{570} as a function of *SZA* and *VZA*. *F*, *sPRI* and *R* were scaled between 0 and 1 before subtraction. Negative values of *SZA* correspond to the cycles acquired before midday, positive - after midday. Negative values of *VZA* represent the backscatter direction, positive - the forward scatter direction within a plane. The points of measurements are marked with white circles. The values between the measurements are linearly interpolated.

deviation of F_{760} from nadir values in the AR plane under high sun elevation (*SZA* = -22°) might be explained by the fact that erectophile canopy does not receive direct light on the leaf surface that much, and, therefore, directional effects are significantly reduced. The distribution of *sPRI* along the SPP and AR measured over rice exhibited a dome-like shape (Figs. 6 and 7), which is driven by the lower fraction of vegetation observed from nadir in an erectophile canopy and the contribution of soil to the reflectance signal (Barton and North, 2001), while the sunlit-shaded fraction controls the shape of the *sPRI* directional response less evidently.

In this work, we measured the reflectance and fluorescence from the top canopy layer, expected to be the one contributing the most to the measured *F* signal (Van Wittenberghe et al., 2015). Due to the complexity of the measurement setup, we could not measure the light distribution and the reflectance/fluorescence for different layers inside the canopy. This would have been useful to characterize the physiological response of the different leaves to different levels of radiation; and potentially to better explain the anisotropic behavior at the top of the canopy. In future campaigns, leaf-level reflectance/fluorescence measurements for different canopy layers, by means of (e.g.) the FLUOWAT leaf clip (Van Wittenberghe et al., 2015) should be performed as well, close in time to the multi-angular measurements.

4.2. Effects of structural parameters on F directional response in the SPP: comparison between observations and simulations

SCOPE forward simulations were useful to disentangle the driving factors of *F* anisotropy in the different crops. Both modelling and experimental results demonstrated that planophile (chickpea), plagiophile (alfalfa) and spherical (grass) canopy types have similar *F* directional response, while the erectophile canopy type (rice) significantly differs. The spectro-directional outputs of the SCOPE model showed *F* distribution characterized by a bowl-like shape with a deep decrease at *VZA* = 0° for the erectophile canopy (Fig. S2). This agrees with the results on bidirectional response of F_{760} in winter wheat (Liu et al., 2016), driven by the presence of high amount of soil fraction, which is mostly visible from nadir and diminishes with higher *VZA*s. Measurements over the rice were complicated by the row structure (Zhao et al., 2015), which, together with relatively wide FOV, might have contributed to the asymmetrical shape of F_{760} directional response, characterized by shifted minimum values towards coldspot in the forward scatter direction (Fig. 9).

Based on SCOPE simulations, the angular distribution of *F* for spherical canopy type also shows a bowl-like shape but with lower anisotropy factor and an evident hotspot in the backscatter direction for $LAI > 3\ m^2\ m^{-2}$ (Fig. S3). For grass (spherical), instead, we observed a

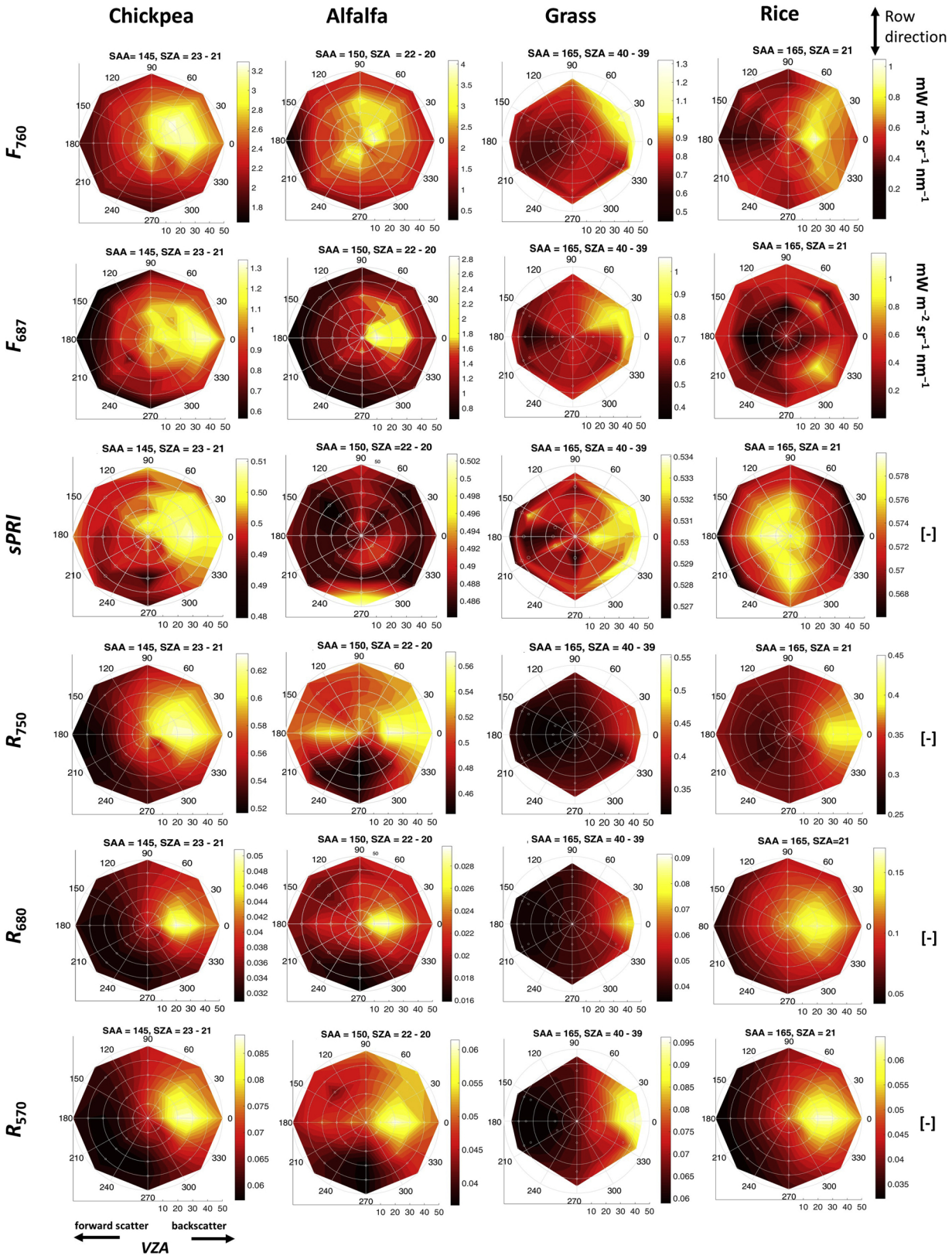

Fig. 8. Polar plots of the angular distribution of F_{760}, F_{687}, *sPRI*, R_{750}, R_{680} and R_{570} measured in chickpea, alfalfa, grass and rice canopies as a function of *VZA* and *RAA*.

well-defined bowl-like shape of F_{760} distribution, but no hotspot (Fig. 9). The absence of the hotspot can be explained by relatively high *sl* (0.1) and low *LAI* (1 $m^2 m^{-2}$), which minimized the width and the magnitude of the hotspot.

Directional responses of *F* measured for alfalfa (plagiophile) and chickpea (planophile) are similar to each other (Fig. 9). This can be explained by comparable *LAI* (7 - 8 $m^2 m^{-2}$) and *sl* (0.01). The shape of the *F* distributions for these species conforms to the modeling results

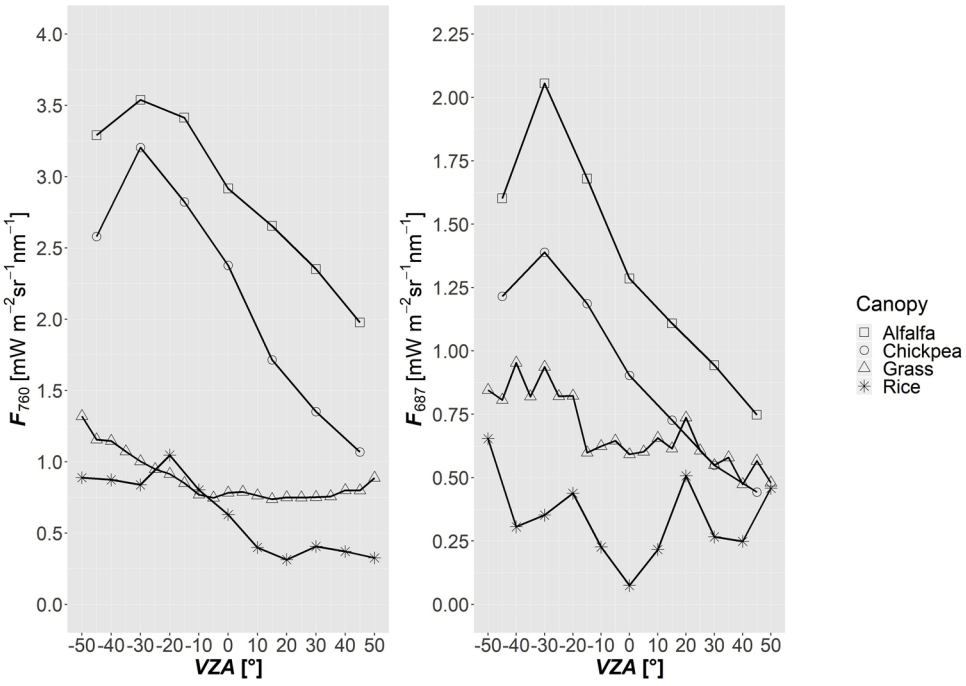

Fig. 9. Angular distribution of F_{760} (left) and F_{687} (right) in the solar principal plane (SPP) as a function of *VZA* for alfalfa, chickpea and rice measured with *SZA* of 22 - 30° and *SAA* of 220 - 230°, and grass measured with *SZA* of 39° and *SAA* of 184°. Negative values of *VZA* represent the backscatter direction, positive - the forward scatter direction within a plane.

(Fig. S3), however, the measured hotspot is wider than the modeled one due to the averaging effect of the sensor's FOV, which integrates the signal over 25° rather than in an infinitesimal solid angle as in SCOPE (Schaepman-Strub et al., 2006). Considering variability within a plane, field observations showed higher *ANIX* compared to modelling results (Tables S1, S9) affected by quicker decrease in the forward scatter direction (Fig. 9). F_{687} directional response for alfalfa and chickpea canopies, which are similar in C_{ab} and *LAI*, exhibited higher difference in

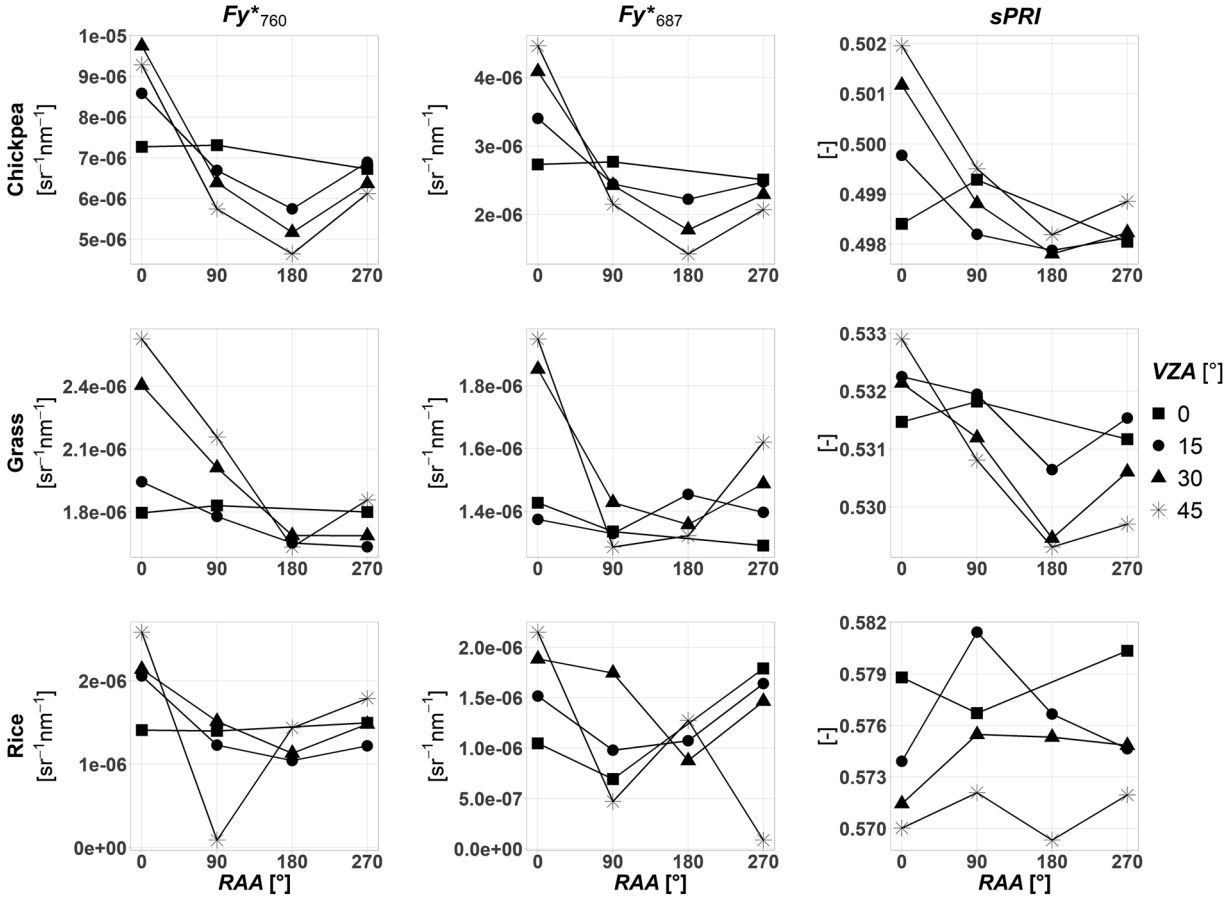

Fig. 10. The daily average values of Fy^*_{760}, Fy^*_{687} and *sPRI* obtained at four *VZA*s (0°, 15°, 30°, 45°) with four *RAA*s (0°, 90°, 18°, 270°) for chickpea (row 1), grass (row 2) and rice (row 3).

absolute values and specifically in the hotspot compared to F_{760}. Having a little higher C_{ab} and a little lower *LAI*, one would expect to observe lower or identical values for F_{687} for alfalfa compared to chickpea due to F_{687} reabsorption. However, the results showed higher values of F_{687} for alfalfa, which might be explained by its heliotropic leaf movements (Walter-Shea et al., 1997; Strub et al., 2003) resulting in the higher fraction of sunlit leaves, especially in the backscatter direction of the SPP.

4.3. Fluorescence apparent yield and sPRI daily variations as a function of VZA and RAA: implications for ground measurements

In this work we performed a quantitative evaluation of the impact of anisotropy on *Fy** and *sPRI*. We found, that for the homogenous and mature canopies (chickpea) off-nadir acquisitions result in lower *Fy** at all *RAA*s except the backscatter direction in the solar principal plane (*RAA* = 0°), where *Fy** increased by 20–67 % compared to nadir acquisitions. For all other *RAA*s (90°, 180°, 270°), *Fy** values measured with the sensor's inclination of 15° decreased by 3–20 %. With higher *VZA*s (*VZA* = 30° - 45°), Fy^*_{760} decreased by 10–35 % and Fy^*_{687} by 10–45 %. The same pattern was observed for *sPRI*, where the biggest discrepancies occurred in the backscatter direction of the SPP at high *VZA*s. Therefore, an optimal setup for continuous measurements of *F* and *PRI* should have a nadir *VZA*, with an acceptable inclination of up to 5–10°, which, in the case of *F* signal measured over grass, results in less than 3% difference. Balzarolo et al. (2011) suggested using oblique viewing angles to increase the footprint of the measurements of vegetation reflectance, however, based on the current analysis we do not recommend adopting this strategy for continuous *F* measurements. For tower installation we foster the use of a sufficiently long horizontal arm that can carry the optical fibers at the necessary distance from the tower structure. When this would not be possible, a correction scheme for the signal directionality should be considered.

Multi-angular observations, like the ones presented here, can help building or validating these correction schemes, as well as properly interpreting remote observations taken under varying solar-view geometries (e.g., at different latitudes within a satellite orbit). Nevertheless, the deployment of field goniometers is demanding and limited to relatively short canopies. In this regard, continuous observations by means of automated, tower-based scanning systems (Leuning et al., 2006; Hilker et al., 2007; Corp et al., 2010) may complement nadir-looking systems towards a complete characterization of the canopy reflectance and fluorescence signals.

5. Conclusions

In this study we present a unique dataset of multi-angular observations of *F*, *R* and *sPRI* over four different vegetated targets measured in two main planes — the SPP and CPP — during a day, as well as the angular distribution of *F*, *R* and *sPRI* over the hemisphere at midday, coupled with SCOPE simulations of spectro-directional response of *F* under varying structural and biochemical parameters.

Radiative transfer theory and observations agreed that the shape of *F* bidirectional distribution is controlled by *LIDF*: a bowl-like shape with a deep decrease at nadir is typical for erectophile canopy type, a smooth bowl-like shape for spherical canopy with $LAI < 3\,m^2\,m^{-2}$, a dome-like shape with a pronounced hotspot for planophile canopy type. The magnitude and the shape of the hotspot is controlled by *LAI* and *sl*: a combination of low *sl* and high *LAI* determines a stronger and more pronounced hotspot effect. Both *F* and *sPRI* showed significant directional variability for all the studied canopies, with the highest *ANIX* of *F* within the SPP observed for rice. F_{687} is characterized by higher anisotropy compared to F_{760} due to prevailing re-absorption process in this spectral region. The *sPRI* directional response is characterized by an increase in the backscatter direction and a decrease in the forward scatter direction driven by different contribution of sunlit-shaded fractions of vegetation to the measured signal.

Overall, for homogenous canopies, off-nadir measurements resulted in lower values of *F* and *sPRI* compared to nadir observations at all *RAA*s except the backscatter direction in the SPP, where, on the contrary, the values were higher. Based on a quantitative evaluation of the impact of canopy anisotropy and solar-view geometry on *F* and *sPRI* spectro-directional response, we recommend maintaining nadir viewing geometry in automated proximal sensing systems, with an acceptable inclination up to 5–10°. Nevertheless, UAV, airborne and satellite observations may be forced by design to observe the target at higher *VZA*s, and under different illumination conditions (i.e. different *SZA*s). In order to properly account for the effects of the canopy anisotropy on *F* and *PRI* observations, a correction scheme should be developed and tested against multi-angular measurements.

The results presented in this study demonstrate that the anisotropic response of *F* and *sPRI* and the corresponding *R* do not totally covary and that the angular configuration plays an important role in relative contribution of *F* and *sPRI* compared to reference *R*.

The characterization of these anisotropic responses along the daily cycle (i.e., under varying *SZA* and *SAA*) may also prove useful for evaluating the plant response to the different relative illumination conditions that appear along long-term time series, within a satellite orbit, or in general for different geographical locations and times within a validation framework.

CRediT authorship contribution statement

Khelvi Biriukova: Conceptualization, Methodology, Formal analysis, Investigation, Data curation, Writing - original draft, Writing - review & editing, Visualization. **Marco Celesti:** Conceptualization, Methodology, Investigation, Writing - original draft, Writing - review & editing, Supervision. **Anton Evdokimov:** Methodology, Investigation, Visualization, Writing - review & editing. **Javier Pacheco-Labrador:** Conceptualization, Writing - review & editing. **Tommaso Julitta:** Methodology, Software, Data curation. **Mirco Migliavacca:** Conceptualization, Writing - review & editing, Resources. **Claudia Giardino:** Resources, Methodology. **Franco Miglietta:** Project administration, Resources, Investigation. **Roberto Colombo:** Project administration, Resources, Writing - review & editing. **Cinzia Panigada:** Conceptualization, Methodology, Investigation, Project administration, Funding acquisition, Supervision. **Micol Rossini:** Conceptualization, Methodology, Writing - original draft, Writing - review & editing, Supervision, Project administration, Funding acquisition.

Declaration of Competing Interest

The authors declare no conflict of interest.

Acknowledgments

This project has received funding from the European Union's Horizon 2020 research and innovation programme under the Marie Skłodowska-Curie grant agreement No 721995. Marco Celesti was supported by a Living Planet Fellowship (ESA/Contract No. 4000125442/18/I-NS) of the European Space Agency.

We thank Martina Anelli, Mirco Boschetti, Gabriele Candiani and Giulia Tagliabue for their support during the campaign in Braccagni; Valentina Picchi for the extraction of chlorophyll content of alfalfa and chickpea; Maria Pilar Martín and Rosario González-Cascón for providing *LAI* and chlorophyll content values for Majadas de Tiétar field site; Sergio Cogliati for providing code for fluorescence SFM retrieval. We also thank Fondazione per il Clima e la Sostenibilità (FCS) for field work support, and Azienda Agricola "Le Rogaie" and "Fattoria Poggetti Vecchi" for hosting the field experiments.

Appendix A. Supplementary data

Supplementary material related to this article can be found, in the online version, at doi:https://doi.org/10.1016/j.jag.2020.102069.

References

Aasen, Helge, Van Wittenberghe, Shari, Medina, Neus Sabater, Damm, Alexander, Goulas, Yves, Wieneke, Sebastian, Hueni, Andreas, et al., 2019. Sun-induced chlorophyll fluorescence II: review of passive measurement setups, protocols, and their application at the leaf to canopy level. Remote Sens. 11 (8), 1–32. https://doi.org/10.3390/rs11080956.

Alonso, Luis, Van Wittenberghe, Shari, Amorós-López, Julia, Vila-Francés, Joan, Gómez-Chova, Luis, Moreno, Jose, 2017. Diurnal cycle relationships between passive fluorescence, PRI and NPQ of vegetation in a controlled stress experiment. Remote Sens. 9 (8). https://doi.org/10.3390/rs9080770.

Balzarolo, M., Anderson, K., Nichol, C., Rossini, M., Vescovo, L., Arriga, N., Wohlfahrt, G., Calvet, J.C., Carrara, A., Cerasoli, S., Cogliati, S., Daumard, F., Eklundh, L., Elbers, J.A., Evrendilek, F., Handcock, R.N., Kaduk, J., Klumpp, K., Longdoz, B., Matteucci, G., Meroni, M., Montagnani, L., Ourcival, J.M., Sanchez-Canete, E.P., Pontailler, J.Y., Juszczak, R., Scholes, B.M., 2011. Ground-based optical measurements at european flux 711 sites: a review of methods, instruments and current controversies. Sensors 11 (8), 7981. https://doi.org/10.3390/s110807954. 7954–712.

Barton, C.V.M., North, P.R.J., 2001. Remote sensing of canopy light use efficiency using the photochemical reflectance index model and sensitivity analysis. Remote Sens. Environ. 78 (3), 264–273. https://doi.org/10.1016/S0034-4257(01)00224-3.

Buschmann, Claus., 2007. Variability and application of the chlorophyll fluorescence emission ratio red/far-red of leaves. Photosyn. Res. 92 (2), 261–271. https://doi.org/10.1007/s11120-007-9187-8.

Campbell, Petya K.E., Huemmrich, Karl F., Middleton, Elizabeth M., Ward, Lauren A., Julitta, Tommaso, Daughtry, Craig S.T., Burkart, Andreas, Russ, Andrew L., Kustas, William P., 2019. Diurnal and seasonal variations in chlorophyll fluorescence associated with photosynthesis at leaf and canopy scales. Remote Sens. 11 (5). https://doi.org/10.3390/rs11050488.

Celesti, Marco, van der Tol, Christiaan, Cogliati, Sergio, Panigada, Cinzia, Yang, Peiqi, Pinto, Francisco, Rascher, Uwe, Miglietta, Franco, Colombo, Roberto, Rossini, Micol, 2018. Exploring the physiological information of sun-induced chlorophyll fluorescence through radiative transfer model inversion. Remote Sens. Environ. 215 (September 2017), 97–108. https://doi.org/10.1016/j.rse.2018.05.013.

Cendrero-Mateo, Pilar, M., Wieneke, Sebastian, Damm, Alexander, Alonso, Luis, Pinto, Francisco, Moreno, Jose, Guanter, Luis, et al., 2019. Sun-induced chlorophyll fluorescence III: benchmarking retrieval methods and sensor characteristics for proximal sensing. Remote Sens. 11 (8). https://doi.org/10.3390/rs11080921.

Cheng, Yen Ben, Middleton, Elizabeth M., Huemmrich, Karl F., Zhang, Qingyuan, Campbell, Petya K.E., Corp, Lawrence A., Russ, Andrew L., Kustas, William P., 2010. Utilizing in situ directional hyperspectral measurements to validate bio-indicator simulations for a corn crop canopy. Ecol. Inform. 5 (5), 330–338. https://doi.org/10.1016/j.ecoinf.2010.03.001.

Cheng, Yen Ben, Middleton, Elizabeth M., Zhang, Qingyuan, Corp, Lawrence A., Dandois, Jonathan, Kustas, William P., 2012. The photochemical reflectance index from directional cornfield reflectances: observations and simulations. Remote Sens. Environ. 124, 444–453. https://doi.org/10.1016/j.rse.2012.05.030.

Cogliati, S., Rossini, M., Julitta, T., Meroni, M., Schickling, A., Burkart, A., Pinto, F., Rascher, U., Colombo, R., 2015a. Continuous and long-term measurements of reflectance and sun-induced chlorophyll fluorescence by using novel automated field spectroscopy systems. Remote Sens. Environ. 164, 270–281. https://doi.org/10.1016/j.rse.2015.03.027.

Cogliati, S., Verhoef, W., Kraft, S., Sabater, N., Alonso, L., Vicent, J., Moreno, J., Drusch, M., Colombo, R., 2015b. Retrieval of sun-induced fluorescence using advanced spectral fitting methods. Remote Sens. Environ. 169, 344–357. https://doi.org/10.1016/j.rse.2015.08.022.

Colombo, Roberto, Celesti, Marco, Bianchi, Remo, Campbell, Petya K.E., Cogliati, Sergio, Cook, Bruce D., Corp, Lawrence A., et al., 2018. Variability of sun-induced chlorophyll fluorescence according to stand age-related processes in a managed loblolly pine forest. Glob. Change Biol. 24 (7), 2980–2996. https://doi.org/10.1111/gcb.14097.

Coops, N.C., Hilker, T., Hall, F.G., Nichol, C.J., Drolet, G.G., 2010. Estimation of light-use efficiency of terrestrial ecosystems from space: a status report. Bioscience 60, 788–797.

Corp, Lawrence A., Cook, Bruce D., Middleton, Elizabeth M., Cheng, Yen Ben, Fred Huemmrich, K., Campbell, Petya K.E., 2010. Fusion: a fully ultraportable system for imaging objects in nature. International Geoscience and Remote Sensing Symposium (IGARSS) 1671–1674. https://doi.org/10.1109/IGARSS.2010.5652788.

Damm, A., Guanter, L., Verhoef, W., Schläpfer, D., Garbari, S., Schaepman, M.E., 2015. Impact of varying irradiance on vegetation indices and chlorophyll fluorescence derived from spectroscopy data. Remote Sens. Environ. 156, 202–215. https://doi.org/10.1016/j.rse.2014.09.031.

Daumard, Fabrice, Champagne, Sbastien, Fournier, Antoine, Goulas, Yves, Ounis, Abderrahmane, Hanocq, Jean Franois, Moya, Ismal, 2010. A field platform for continuous measurement of canopy fluorescence. Ieee Trans. Geosci. Remote. Sens. 48 (9), 3358–3368. https://doi.org/10.1109/TGRS.2010.2046420.

De Wit, C.T., 1965. Photosynthesis of leaf canopies. Agricultural Research Reports 663. pp. 1–54. https://doi.org/10.2172/4289474.

Demmig-Adams, B., Adams, W.W., 1992. Photoprotection and other responses of plants to high light stress. Annu. Rev. Plant Physiol. Plant Mol. Biol. 43 (1), 599–626. https://doi.org/10.1146/annurev.pp.43.060192.003123.

Drolet, Guillaume G., Huemmrich, Karl F., Hall, Forrest G., Middleton, Elizabeth M., Andrew Black, T., Barr, Alan G., Margolis, Hank A., 2005. A MODIS-derived photochemical reflectance index to detect inter-annual variations in the photosynthetic light-use efficiency of a boreal deciduous forest. Remote Sens. Environ. 98 (2–3), 212–224. https://doi.org/10.1016/j.rse.2005.07.006.

Drusch, Matthias, Moreno, Jose, Umberto Del Bello, Raffaella Franco, Goulas, Yves, Huth, Andreas, Kraft, Stefan, et al., 2017. The FLuorescence EXplorer Mission Concept-ESA's Earth Explorer 8. Ieee Trans. Geosci. Remote. Sens. 55 (3), 1273–1284. https://doi.org/10.1109/TGRS.2016.2621820.

Filella, Iolanda, Amaro, Teo, Araus, Jose Luis, Peñuelas, Josep, 1996. Relationship between photosynthetic radiation-use efficiency of barley canopies and the photochemical reflectance index (PRI). Physiol. Plant. 96 (2), 211–216. https://doi.org/10.1111/j.1399-3054.1996.tb00204.x.

Fournier, A., Daumard, F., Champagne, S., Ounis, A., Goulas, Y., Moya, I., 2012. Effect of canopy structure on sun-induced chlorophyll fluorescence. ISPRS J. Photogramm. Remote. Sens. 68 (1), 112–120. https://doi.org/10.1016/j.isprsjprs.2012.01.003.

Frankenberg, C., Berry, J., 2018. Solar induced chlorophyll fluorescence: origins, relation to photosynthesis and retrieval. Compr. Remote Sens. 3, 143–162. https://doi.org/10.1016/b978-0-12-409548-9.10632-3.

Gamon, J.A., Peñuelas, J., Field, C.B., 1992. A narrow-waveband spectral index that tracks diurnal changes in photosynthetic efficiency. Remote Sens. Environ. 41 (1), 35–44. https://doi.org/10.1016/0034-4257(92)90059-S.

Gamon, J.A., Rahman, A.F., Dungan, J.L., Schildhauer, M., Huemmrich, K.F., 2006. Spectral network (SpecNet)-what is it and why do we need it? Remote Sens. Environ. 103 (3), 227–235. https://doi.org/10.1016/j.rse.2006.04.003.

Garbulsky, Martín F., Peñuelas, Josep, Gamon, John, Inoue, Yoshio, Filella, Iolanda, 2011. The photochemical reflectance index (PRI) and the remote sensing of leaf, canopy and ecosystem radiation use efficiencies. A review and meta-analysis. Remote Sens. Environ. 115 (2), 281–297. https://doi.org/10.1016/j.rse.2010.08.023.

Garbulsky, Martín F., Peñuelas, Josep, Ogaya, Romà, Filella, Iolanda, 2013. Leaf and stand-level carbon uptake of a mediterranean forest estimated using the satellite-derived reflectance indices EVI and PRI. Int. J. Remote Sens. 34 (4), 1282–1296. https://doi.org/10.1080/01431161.2012.718457.

Garzonio, Roberto, Di Mauro, Biagio, Colombo, Roberto, Cogliati, Sergio, 2017. Surface reflectance and sun-induced fluorescence spectroscopy measurements using a small hyperspectral UAS. Remote Sens. 9 (5), 472. https://doi.org/10.3390/rs9050472.

Giardino, C., Brivio, P.A., 2003. The application of a dedicated device to acquire bidirectional reflectance factors over natural surfaces. Int. J. Remote Sens. 24 (14), 2989–2995. https://doi.org/10.1080/0143116031000094782.

Gitelson, A.A., Buschmann, C., Lichtenthaler, H.K., 1999. The chlorophyll fluorescence ratio F735/F700 as an accurate measure of chlorophyll content in plants. Remote Sens. Environ. 69, 296–302.

Gonzalez-Cascón, R., Martín, M.P., 2018. Protocol for Pigment Content Quantification in Herbaceous Covers: Sampling and Analysis. protocols.io. dx.doi.org/10.17504/protocols.io.qs6dwhe. .

Grace, J., Nichol, C., Disney, M., Lewis, P., Quaife, T., Bowyer, P., 2007. Can we measure terrestrial photosynthesis from space directly, using spectral reflectance and fluorescence? Glob. Change Biol. 13, 1484–1497.

Guan, Kaiyu, Berry, Joseph A., Zhang, Yongguang, Joiner, Joanna, Guanter, Luis, Badgley, Grayson, Lobell, David B., 2016. Improving the monitoring of crop productivity using spaceborne solar-induced fluorescence. Glob. Change Biol. 22 (2), 716–726. https://doi.org/10.1111/gcb.13136.

Hall, Forrest G., Hilker, Thomas, Coops, Nicholas C., Lyapustin, Alexei, Huemmrich, Karl F., Middleton, Elizabeth, Margolis, Hank, Drolet, Guillaume, Andrew Black, T., 2008. Multi-angle remote sensing of forest light use efficiency by observing PRI variation with canopy shadow fraction. Remote Sens. Environ. 112 (7), 3201–3211. https://doi.org/10.1016/j.rse.2008.03.015.

Hall, Forrest G., Hilker, Thomas, Coops, Nicholas C., 2011. PHOTOSYNSAT, photosynthesis from space: theoretical foundations of a satellite concept and validation from tower and spaceborne data. Remote Sens. Environ. 115 (8), 1918–1925. https://doi.org/10.1016/j.rse.2011.03.014.

Hilker, Thomas, Coops, Nicholas C., Nesic, Zoran, Wulder, Michael A., Black, Andrew T., 2007. Instrumentation and approach for unattended year round tower based measurements of spectral reflectance. Comput. Electron. Agric. 56 (1), 72–84. https://doi.org/10.1016/j.compag.2007.01.003.

Hilker, Thomas, Coops, Nicholas C., Hall, Forrest G., Andrew Black, T., Wulder, Michael A., Nesic, Zoran, Krishnan, Praveena, 2008. Separating physiologically and directionally induced changes in PRI using BRDF models. Remote Sens. Environ. 112 (6), 2777–2788. https://doi.org/10.1016/j.rse.2008.01.011.

Hilker, Thomas, Nesic, Zoran, Coops, Nicholas C., Lessard, Dominic, 2010a. A new, automated, multiangular radiometer instrument for tower-based observations of canopy reflectance (AMSPEC II). Instrum. Sci. Technol. 38 (5), 319–340. https://doi.org/10.1080/10739149.2010.508357.

Hilker, Thomas, Hall, Forrest G., Coops, Nicholas C., Lyapustin, Alexei, Wang, Yujie, Nesic, Zoran, Grant, Nick, et al., 2010b. Remote sensing of photosynthetic light-use efficiency across two forested biomes: spatial scaling. Remote Sens. Environ. 114 (12), 2863–2874. https://doi.org/10.1016/j.rse.2010.07.004.

Hilker, Thomas, Gitelson, Anatoly, Coops, Nicholas C., Hall, Forrest G., Andrew Black, T., 2011. Tracking plant physiological properties from multi-angular tower-based remote sensing. Oecologia 165 (4), 865–876. https://doi.org/10.1007/s00442-010-1901-0.

Julitta, T., Burkart, A., Colombo, R., Rossini, M., Schickling, A., Migliavacca, M., Cogliati, S., Wutzler, T., Rascher, U., 2017. Accurate measurements of fluorescence in the O2A 855 and O2B band using the FloX spectroscopy system – results and prospects. In:

Potsdam 856 GHG Workshop. From Photosystems to Ecosystems. 24-26 October 2017, Postdam, 857. Germany.
Jupp, D.L.B., Strahler, A.H., 1991. A hotspot model for leaf canopies. Remote Sens. Environ. 38, 193–210.
Knyazikhin, Yuri, Schull, Mitchell A., Stenberg, Pauline, Mõttus, Matti, Rautiainen, Miina, Yang, Yan, Marshak, Alexander, et al., 2013. Hyperspectral remote sensing of foliar nitrogen content. Proc. Natl. Acad. Sci. U. S. A. 110 (3), 1–8. https://doi.org/10.1073/pnas.1210196109.
Köhler, Philipp, Guanter, Luis, Kobayashi, Hideki, Walther, Sophia, Yang, Wei, 2018. Assessing the potential of sun-induced fluorescence and the canopy scattering coefficient to track large-scale vegetation dynamics in Amazon forests. Remote Sens. Environ. 204 (April 2016), 769–785. https://doi.org/10.1016/j.rse.2017.09.025.
Krause, G.H., Weis, E., 1991. Chlorophyll fluorescence and photosynthesis: the basics. Annu. Rev. Plant Physiol. Plant Mol. Biol. 42 (1), 313–349. https://doi.org/10.1146/annurev.pp.42.060191.001525.
Leuning, Ray, Hughes, Dale, Daniel, Paul, Coops, Nicholas C., Newnham, Glenn, 2006. A multi-angle spectrometer for automatic measurement of plant canopy reflectance spectra. Remote Sens. Environ. 103 (3), 236–245. https://doi.org/10.1016/j.rse.2005.06.016.
Lichtenthaler, Hartmut K., Buschmann, Claus, 2001. Chlorophylls and carotenoids: measurement and characterization by UV-vis spectroscopy. Curr. Protoc. Food Anal. Chem. F4.3.1-F4 (Suppl. 1), 1–8.
Liu, Liangyun, Liu, Xinjie, Wang, Zhihui, Zhang, Bing, 2016. Measurement and analysis of bidirectional SIF emissions in wheat canopies. IEEE Trans. Geosci. Remote. Sens. 54 (5), 2640–2651. https://doi.org/10.1109/TGRS.2015.2504089.
Luus, K.A., Commane, R., Parazoo, N.C., Benmergui, J., Euskirchen, E.S., Frankenberg, C., Joiner, J., et al., 2017. Tundra photosynthesis captured by satellite-observed solar-induced chlorophyll fluorescence. Geophys. Res. Lett. 44 (3), 1564–1573. https://doi.org/10.1002/2016GL070842.
Meroni, M., Colombo, R., 2006. Leaf level detection of solar induced chlorophyll fluorescence by means of a subnanometer resolution spectroradiometer. Remote Sens. Environ. 103 (4), 438–448. https://doi.org/10.1016/j.rse.2006.03.016.
Meroni, M., Rossini, M., Guanter, L., Alonso, L., Rascher, U., Colombo, R., Moreno, J., 2009. Remote sensing of solar-induced chlorophyll fluorescence: review of methods and applications. Remote Sens. Environ. 113 (10), 2037–2051. https://doi.org/10.1016/j.rse.2009.05.003.
Meroni, M., Busetto, L., Colombo, R., Guanter, L., Moreno, J., Verhoef, W., 2010. Performance of spectral fitting methods for vegetation fluorescence quantification. Remote Sens. Environ. 114 (2), 363–374. https://doi.org/10.1016/j.rse.2009.09.010.
Middleton, Elizabeth M., Cheng, Yen Ben, Hilker, Thomas, Andrew Black, T., Krishnan, Praveena, Coops, Nicholas C., Huemmrich, Karl Fred, 2009a. Linking foliage spectral responses to canopy-level ecosystem photosynthetic light-use efficiency at a Douglas-Fir Forest in Canada. Can. J. Remote. Sens. 35 (2), 166–188. https://doi.org/10.5589/m09-008.
Middleton, E.M., Cheng, Y.-B., Corp, L.A., Huemmrich, K.F., Campbell, P.K.E., Zhang, Q.-Y., Kustas, W.P., Russ, A.L., 2009b. Diurnal and seasonal dynamics of canopy-level solar-induced chlorophyll fluorescence and spectral reflectance indices in a cornfield. 6th European Association of Remote Sensing Laboratories (EARSeL) SIG Imaging SpectroscopyWorkshop. https://pdfs.semanticscholar.org/d01b/193b4a25cc6c849dd51966a46f00bc4d9ca8.pdf.
Middleton, Elizabeth M., Cheng, Yen Ben, Corp, Lawrence A., Campbell, Petya K.E., Fred Huemmrich, K., Zhang, Qingyuan, Kustas, William P., 2012. Canopy level chlorophyll fluorescence and the PRI in a cornfield. International Geoscience and Remote Sensing Symposium (IGARSS) 7117–7120. https://doi.org/10.1109/IGARSS.2012.6352022.
Middleton, E.M., Huemmrich, K.F., Landis, D.R., Black, T.A., Barr, A.G., McCaughey, J.H., 2016. Photosynthetic efficiency of northern forest ecosystems using a MODIS-Derived photochemical reflectance index (PRI). Remote Sens. Environ. 187, 345–366. https://doi.org/10.1016/j.rse.2016.10.021.
Middleton, Elizabeth M., Rascher, Uwe, Corp, Lawrence A., Fred Huemmrich, K., Cook, Bruce D., Noormets, Asko, Schickling, Anke, et al., 2017. The 2013 FLEX-US airborne campaign at the parker tract loblolly pine plantation in North Carolina, USA. Remote Sens. 9 (6), 1–31. https://doi.org/10.3390/rs9060612.
Middleton, E.M., Huemmrich, K.F., Zhang, Q., Campbell, P.K.E., Landis, D.R., 2018. Photosynthetic efficiency and vegetation stress, chap. 5. In: 2nd edition. In: Thenkabail, P.S., Lyon, J.G., Huete, A. (Eds.), Hyperspectral Remote Sensing of Vegetation Vol. III. Biophysical and Biochemical Characterization and Plant Species Studies Taylor & Francis, New York, pp. 133–179.
Migliavacca, Mirco, Perez-Priego, Oscar, Rossini, Micol, El-Madany, Tarek S., Moreno, Gerardo, van der Tol, Christiaan, Rascher, Uwe, et al., 2017. Plant functional traits and canopy structure control the relationship between photosynthetic CO 2 uptake and far-red sun-induced fluorescence in a Mediterranean grassland under different nutrient availability. New Phytol. 214 (3), 1078–1091. https://doi.org/10.1111/nph.14437.
Mohammed, Gina H., Colombo, Roberto, Middleton, Elizabeth M., Rascher, Uwe, van der Tol, Christiaan, Nedbal, Ladislav, Goulas, Yves, et al., 2019. Remote sensing of solar-induced chlorophyll fluorescence (SIF) in vegetation: 50 years of progress. Remote Sens. Environ. 231 (February), 111177. https://doi.org/10.1016/j.rse.2019.04.030.
Müller, P., Li, X.P., Niyogi, K.K., 2001. Non-photochemical quenching. a response to excess light energy. Plant Physiol. 125 (4), 1558. https://doi.org/10.1104/pp.125.4.1558. 66.
Pacheco-Labrador, Javier, Hueni, Andreas, Mihai, Laura, Sakowska, Karolina, Julitta, Tommaso, Kuusk, Joel, Sporea, Dan, et al., 2019. Sun-induced chlorophyll fluorescence I: instrumental considerations for proximal spectroradiometers. Remote Sens. 11 (8), 1–29. https://doi.org/10.3390/rs11080960.
Paul-Limoges, Eugénie, Damm, Alexander, Hueni, Andreas, Liebisch, Frank, Eugster, Werner, Schaepman, Michael E., Buchmann, Nina, 2018. Effect of environmental conditions on sun-induced fluorescence in a mixed forest and a cropland. Remote Sens. Environ. 219 (November 2017), 310–323. https://doi.org/10.1016/j.rse.2018.10.018.
Peñuelas, Josep, Eielella, Iolanda, Gamon, John A., 1995. Assessment of photosynthetic radiation-use efficiency with spectral reflectance. New Phytol. 291–296. https://doi.org/10.1039/c0cc01272f.
Perez-Priego, O., Guan, J., Rossini, M., Fava, F., Wutzler, T., Moreno, G., Carvalhais, N., et al., 2015. Sun-induced chlorophyll fluorescence and photochemical reflectance index improve remote-sensing gross primary production estimates under varying nutrient availability in a typical Mediterranean Savanna ecosystem. Biogeosciences 12 (21), 6351–6367. https://doi.org/10.5194/bg-12-6351-2015.
Pinto, Francisco, Müller-Linow, Mark, Schickling, Anke, Pilar Cendrero-Mateo, M., Ballvora, Agim, Rascher, Uwe, 2017. Multiangular observation of canopy sun-induced chlorophyll fluorescence by combining imaging spectroscopy and stereoscopy. Remote Sens. 9 (5). https://doi.org/10.3390/rs9050415.
Porcar-Castell, Albert, Tyystjärvi, Esa, Atherton, Jon, van der Tol, Christiaan, Flexas, Jaume, Pfündel, Erhard E., Moreno, Jose, Frankenberg, Christian, Berry, Joseph A., 2014. Linking chlorophyll *a* fluorescence to photosynthesis for remote sensing applications: mechanisms and challenges. J. Exp. Bot. 65 (15), 4065–4095. https://doi.org/10.1093/jxb/eru191.
Porcar-Castell, A., Mac Arthur, A., Rossini, M., Eklundh, L., Pacheco-Labrador, J., Anderson, K., Balzarolo, M., et al., 2015. EUROSPEC: at the interface between remote-sensing and ecosystem CO2flux measurements in Europe. Biogeosciences 12 (20), 6103–6124. https://doi.org/10.5194/bg-12-6103-2015.
Rahman, Abdullah F., Gamon, John A., Fuentes, David A., Roberts, Dar A., Prentiss, Dylan, 2001. Modeling spatially distributed ecosystem flux of boreal forest using hyperspectral indices from AVIRIS imagery. J. Geophys. Res. Atmos. 106 (D24), 33579–33591. https://doi.org/10.1029/2001JD900157.
Rascher, U., Agati, G., Alonso, L., Cecchi, G., Champagne, S., Colombo, R., Damm, A., et al., 2009. CEFLES2: the remote sensing component to quantify photosynthetic efficiency from the leaf to the region by measuring sun-induced fluorescence in the oxygen absorption bands. Biogeosciences 6 (7), 1181–1198. https://doi.org/10.5194/bg-6-1181-2009.
Rascher, U., Alonso, L., Burkart, A., Cilia, C., Cogliati, S., Colombo, R., Damm, A., et al., 2015. Sun-induced fluorescence – a new probe of photosynthesis: first maps from the imaging spectrometer HyPlant. Glob. Change Biol. 21 (12), 4673–4684. https://doi.org/10.1111/gcb.13017.
Rossini, M., Meroni, M., Migliavacca, M., Manca, G., Cogliati, S., Busetto, L., Picchi, V., Cescatti, A., Seufert, G., Colombo, R., 2010. High resolution field spectroscopy measurements for estimating gross ecosystem production in a rice field. Agric. For. Meteorol. 150, 1283–1296.
Rossini, M., Fava, F., Cogliati, S., Meroni, M., Marchesi, A., Panigada, C., Giardino, C., et al., 2013. Assessing canopy PRI from airborne imagery to map water stress in maize. ISPRS J. Photogramm. Remote. Sens. 86, 168–177. https://doi.org/10.1016/j.isprsjprs.2013.10.002.
Rossini, M., Nedbal, L., Guanter, L., Ač, A., Alonso, L., Burkart, A., Cogliati, S., et al., 2015. Red and far red sun-induced chlorophyll fluorescence as a measure of plant photosynthesis. Geophys. Res. Lett. 42 (6), 1632–1639. https://doi.org/10.1002/2014GL062943.
Rossini, Micol, Meroni, Michele, Celesti, Marco, Cogliati, Sergio, Julitta, Tommaso, Panigada, Cinzia, Rascher, Uwe, van der Tol, Christiaan, Colombo, Roberto, 2016. Analysis of red and far-red sun-induced chlorophyll fluorescence and their ratio in different canopies based on observed and modeled data. Remote Sens. 8 (5). https://doi.org/10.3390/rs8050412.
Roujean, J.L., Leroy, M., Deschamps, P.Y., 1992. A bidirectional reflectance model of the earth's surface for the correction of remote sensing data. J. Geophys. Res. 97 (D18), 20. https://doi.org/10.1029/92jd01411. 455-20,468.
Sandmeier, St, Müller, Ch, Hosgood, B., Andreoli, G., 1998. Physical mechanisms in hyperspectral BRDF data of grass and watercress. Remote Sens. Environ. 66 (2), 222–233. https://doi.org/10.1016/S0034-4257(98)00060-1.
Schaepman-Strub, G., Schaepman, M.E., Painter, T.H., Dangel, S., Martonchik, J.V., 2006. Reflectance quantities in optical remote sensing-definitions and case studies. Remote Sens. Environ. 103 (1), 27–42. https://doi.org/10.1016/j.rse.2006.03.002.
Schickling, Anke, Matveeva, Maria, Damm, Alexander, Schween, Jan H., Wahner, Andreas, Graf, Alexander, Crewell, Susanne, Rascher, Uwe, 2016. Combining sun-induced chlorophyll fluorescence and photochemical reflectance index improves diurnal modeling of gross primary productivity. Remote Sens. 8 (7). https://doi.org/10.3390/rs8070574.
Soudani, Kamel, Hmimina, Gabriel, Dufrêne, Eric, Berveiller, Daniel, Delpierre, Nicolas, Ourcival, Jean Marc, Rambal, Serge, Joffre, Richard, 2014. Relationships between photochemical reflectance index and light-use efficiency in deciduous and evergreen broadleaf forests. Remote Sens. Environ. 144, 73–84. https://doi.org/10.1016/j.rse.2014.01.017.
Stagakis, Stavros, Markos, Nikos, Sykioti, Olga, Kyparissis, Aris, 2014. Tracking seasonal changes of leaf and canopy light use efficiency in a Phlomis Fruticosa Mediterranean Ecosystem using field measurements and multi-angular satellite hyperspectral imagery. ISPRS J. Photogramm. Remote. Sens. 97, 138–151. https://doi.org/10.1016/j.isprsjprs.2014.08.012.
Strub, Gabriela, Schaepman, Michael E., Knyazikhin, Yuri, Itten, Klaus I., 2003. Evaluation of spectrodirectional alfalfa canopy data acquired during DAISEX'99. IEEE Trans. Geosci. Remote. Sens. 41 (5 Part 1), 1034–1042. https://doi.org/10.1109/TGRS.2003.811555.
Sun, Ying, Fu, Rong, Dickinson, Robert, Joiner, Joanna, Frankenberg, Christian, Gu, Lianhong, Xia, Youlong, Fernando, Nelun, 2015. Drought onset mechanisms revealed by satellite solar-induced chlorophyll fluorescence: insights from two contrasting

extreme events. J. Geophys. Res. G: Biogeosci. 120 (11), 2427–2440. https://doi.org/10.1002/2015JG003150.

Sun, Ying, Frankenberg, Christian, Jung, Martin, Joiner, Joanna, Guanter, Luis, Köhler, Philipp, Magney, Troy, 2018. Overview of solar-induced chlorophyll fluorescence (SIF) from the orbiting carbon observatory-2: retrieval, cross-mission comparison, and global monitoring for GPP. Remote Sens. Environ. 209 (February), 808–823. https://doi.org/10.1016/j.rse.2018.02.016.

van der Tol, C., Verhoef, W., Timmermans, J., Verhoef, A., Su, Z., 2009. An integrated model of soil-canopy spectral radiance observations, photosynthesis, fluorescence. Biogeosciences Discuss. 6 (3), 6025–6075. https://doi.org/10.5194/bgd-6-6025-2009.

van Wittenberghe, Shari, Alonso, Luis, Verrelst, Jochem, Moreno, José, Samson, Roeland, 2015. Bidirectional sun-induced chlorophyll fluorescence emission is influenced by leaf structure and light scattering properties – a bottom-up approach. Remote Sens. Environ. 158 (2015), 169–179. https://doi.org/10.1016/j.rse.2014.11.012.

Verhoef, Wout, 1998. Theory of Radiative Transfer Models Applied in Optical Remote Sensing of Vegetation Canopies. Wageningen Agricultural University https://doi.org/ISBNL 90-5485-804-4.

Vilfan, Nastassia, van der Tol, Christiaan, Yang, Peiqi, Wyber, Rhys, Malenovský, Zbyněk, Robinson, Sharon A., Verhoef, Wouter, 2018. Extending fluspect to simulate xanthophyll driven leaf reflectance dynamics. Remote Sens. Environ. 211 (March), 345–356. https://doi.org/10.1016/j.rse.2018.04.012.

Walter-Shea, E.A., Privette, J., Cornell, D., Mesarch, M.A., Hays, C.J., 1997. Relations between directional spectral vegetation indices and leaf area and absorbed radiation in Alfalfa. Remote Sens. Environ. 61 (1), 162–177. https://doi.org/10.1016/S0034-4257(96)00250-7.

Wohlfahrt, G., Gerdel, K., Migliavacca, M., Rotenberg, E., Tatarinov, F., Müller, J., Hammerle, A., Julitta, T., Spielmann, F.M., Yakir, D., 2018. Sun-induced fluorescence and gross primary productivity during a heat wave. Sci. Rep. 8 (1), 1–9. https://doi.org/10.1038/s41598-018-32602-z.

Yang, Peiqi, van der Tol, Christiaan, 2018. Linking canopy scattering of far-red sun-induced chlorophyll fluorescence with reflectance. Remote Sens. Environ. 209 (May), 456–467. https://doi.org/10.1016/j.rse.2018.02.029.

Yang, Xi, Tang, Jianwu, Mustard, John F., Lee, Jung Eun, Rossini, Micol, Joiner, Joanna, William Munger, J., Kornfeld, Ari, Richardson, Andrew D., 2015. Solar-induced chlorophyll fluorescence that correlates with canopy photosynthesis on diurnal and seasonal scales in a temperate deciduous forest. Geophys. Res. Lett. 42 (8), 2977–2987. https://doi.org/10.1002/2015GL063201.

Yang, Hualei, Yang, Xi, Zhang, Yongguang, Heskel, Mary A., Xiaoliang, Lu, William Munger, J., Sun, Shucun, Tang, Jianwu, 2017. Chlorophyll fluorescence tracks seasonal variations of photosynthesis from leaf to canopy in a temperate forest. Glob. Change Biol. 23 (7), 2874–2886. https://doi.org/10.1111/gcb.13590.

Yang, Xi, Shi, Hanyu, Stovall, Atticus, Guan, Kaiyu, Miao, Guofang, Zhang, Yongguang, Zhang, Yao, Xiao, Xiangming, Ryu, Youngryel, Lee, Jung Eun, 2018. FluoSpec 2—an automated field spectroscopy system to monitor canopy solar-induced fluorescence. Sensors 18 (7). https://doi.org/10.3390/s18072063.

Zarco-Tejada, P.J., 2000. "Hyperspectral Remote Sensing of Closed Forest Canopies: Estimation of Chlorophyll Fluorescence and Pigment Content." PhD diss. York University Toronto.

Zarco-Tejada, P.J., González-Dugo, V., Berni, J.A.J., 2012. Fluorescence, temperature and narrow-band indices acquired from a UAV platform for water stress detection using a micro-hyperspectral imager and a thermal camera. Remote Sens. Environ. 117, 322–337. https://doi.org/10.1016/j.rse.2011.10.007.

Zhang, Qian, Ju, Weimin, Chen, Jing M., Wang, Huimin, Yang, Fengting, Fan, Weiliang, Huang, Qing, et al., 2015. Ability of the photochemical reflectance index to track light use efficiency for a sub-tropical planted coniferous forest. Remote Sens. 7 (12), 16938–16962. https://doi.org/10.3390/rs71215860.

Zhang, Qian, Chen, Jing M., Ju, Weimin, Wang, Huimin, Qiu, Feng, Yang, Fengting, Fan, Weiliang, et al., 2017. Improving the ability of the photochemical reflectance index to track canopy light use efficiency through differentiating sunlit and shaded leaves. Remote Sens. Environ. 194, 1–15. https://doi.org/10.1016/j.rse.2017.03.012.

Zhao, Feng, Gu, Xingfa, Verhoef, Wout, Wang, Qiao, Yu, Tao, Liu, Qiang, Huang, Huaguo, Qin, Wenhan, Chen, Liangfu, Zhao, Huijie, 2010. A spectral directional reflectance model of row crops. Remote Sens. Environ. 114 (2), 265–285. https://doi.org/10.1016/j.rse.2009.09.018.

Zhao, Feng, Li, Yuguang, Dai, Xu, Verhoef, Wout, Guo, Yiqing, Shang, Hong, Gu, Xingfa, Huang, Yanbo, 2015. Simulated impact of sensor field of view and distance on field measurements of bidirectional reflectance factors for row crops. Remote Sens. Environ. 156, 129–142. https://doi.org/10.1016/j.rse.2014.09.011.